MULTI-USER COMMUNICATION OVER HYBRID FSO UWB CHANNELS

by

Erman Çağıral

B.S, Electronics and Electrical Engineering, Dokuz Eylül University, 2007

Submitted to the Institute for Graduate Studies in
Science and Engineering in partial fulfillment of
the requirements for the degree of
Master of Science

Graduate Program in FBE Program for which the Thesis is Submitted
Boğaziçi University
2010

MULTI-USER COMMUNICATION OVER HYBRID FSO UWB CHANNELS

APPROVED BY:

Assist. Prof. Mutlu Koca (Thesis Supervisor)	.....
Prof. Hakan Deliç	.....
Prof. Naci İnci	.....

DATE OF APPROVAL: 29.07.2010

ACKNOWLEDGEMENTS

I would like to thank to my supervisor Assist. Prof. Mutlu Koca for his guidance to develop my understanding on advanced communications and to prepare the thesis, to my advisor Emin Anarım for his help during my master education,to Naci İnci for his help to gain knowledge on optical systems and to Hakan Deliç for participating in my thesis committee.

My Friend Kemal Davaslioglu, for his dedication, support, and friendship.

Last but not least to Nagihan Taşçı for her moral support during my master education and to my family for their eternal support.

This thesis is supported by the Scientific and Technological Research Council of Turkey (TUBITAK) under the grant number 105E077.

ABSTRACT

MULTI-USER COMMUNICATION OVER HYBRID FSO UWB CHANNELS

UWB communication provides high data rates with a simple signal model over RF channels up to 10 meters. In literature, several studies have been done to generate and transmit UWB signals over optical carrier via fiber cables. Low noise and attenuation values of fiber cables makes UWB over fiber technology best candidate for inter city UWB signal distribution. On the other hand, high deployment costs is the weakness point of the fiber cables especially for the inner city distribution. In this thesis we have proposed a system to carry UWB signals over free space optic channel to fill the gap between fiber and RF communication. Performance results show that proposed system is able to provide reliable data communication for open air conditions. Moreover, different receiver structures are analyzed with multiuser interference since the system purpose is inner city data distribution. Multiuser performance is evaluated for different fading regimes, synchronous-asynchronous user cases and dependent-independent multiuser fading environments.

ÖZET

UWB FSO KARMA KANALLAR ÜZERİNDEN ÇOK KULLANICILI İLETİŞİM

Yüksek frekanslı UWB sistemler yüksek veri hızlarını basit sinyal modeli ile fakat 10 metre ile sınırlı dar bir alanda sunmaktadır. Literatürde, UWB sinyallerin optik ortamda yaratılıp fiber kablolar aracılığı ile dağıtılmasını inceleyen çeşitli çalışmalar mevcuttur. Düşük gürültü ve zayıflama oranları fiber kabloları şehirlerarası UWB dağıtımı için en iyi aday yapmaktadır. Öte yandan, yüksek kurulum ücretleri özellilkle şehir içi iletişim için fiber kabloların en zayıf özelliğidir. Bu tezde UWB sinayalleri optik olarak boşlukta taşıyabilecek yeni bir sistem önerilmiştir. Önerilen sistemin UWB sinyallerin taşınması açısından fiber kablolar ve yüksek frekans arasındak boşluğu doldurması beklenmektedir. İncelenen başarım sonuçları UWB sinyallerin boşlukta güvenilir bir şekilde taşınabildiğini göstermiştir. Ayrıca sistemin şehir içi veri transferini amaçlıyor olması nedeni ile çok kullanıcı girişimine karşı farklı alıcı tipleri incelenmiştir. Çok kullanıcı başarımı eşzamanlı-eşzamasız kullanıcı durumları, farklı sönümlenme tipleri ve bağımlı-bağımsız sönümlenme ortamları için analiz edilmiştir.

TABLE OF CONTENTS

ACKNOWLEDGEMENTS . . . iii
ABSTRACT . . . iv
ÖZET . . . v
LIST OF FIGURES . . . viii
LIST OF TABLES . . . xi
LIST OF SYMBOLS/ABBREVIATIONS . . . xii
1. INTRODUCTION . . . 1
1.1. Thesis Outline . . . 3
2. Free-Space Optical Communications . . . 4
2.1. Free-Space Optical Channel Characteristics . . . 6
2.1.1. Divergence . . . 6
2.1.2. Absorption . . . 7
2.1.3. Scattering . . . 7
2.1.4. Turbulence . . . 8
2.1.5. Displacement . . . 8
2.2. Atmospheric Turbulence . . . 8
2.2.1. Weak Turbulence . . . 9
2.2.2. Moderate Turbulence . . . 11
2.2.3. Strong Turbulence . . . 12
2.3. Ultra Wideband Signal . . . 12
2.3.1. Monocycle Waveforms . . . 14
2.3.2. Modulation Schemas . . . 16
2.3.3. Multiple-Access Techniques . . . 18
3. UWB over FSO . . . 21
3.1. Generation methods . . . 21
3.1.1. Optical impulse radio (IR) system . . . 22
3.1.2. FBG-based Approach . . . 22
3.2. Error performance . . . 23
3.2.1. Error performance under weak turbulence . . . 27

3.2.2. Error performance under moderate turbulence 27
3.2.3. Error performance under strong turbulence 28
3.3. Simulation Results 28
4. Multiuser Detection of IR FSO links 30
4.1. Single User Matched Filter Detection 31
4.1.1. Gauss Model 34
4.1.2. Accurate model 37
4.1.3. Synchronous gauss model 39
4.2. Synchronous Decorrelating Detection 42
4.3. Simulation Results 43
5. CONCLUSIONS 47
APPENDIX A: DERIVATION OF EQUATION (3.12) 48
REFERENCES 49

LIST OF FIGURES

Figure 2.1. Standard deviation of the log-amplitude fluctuation versus propagation distance for a plane wave 10

Figure 2.2. FCC spectral mask for UWB communication 13

Figure 2.3. Gaussian pulse 15

Figure 2.4. Gaussian monocycle 15

Figure 2.5. Gaussian doublet 16

Figure 2.6. Pulse Position Modulation Structure 17

Figure 2.7. Pulse position for two consecutive frames of TH-PPM modulation with $c_n = 1, c_{n+1} = 0$ and $d_n = 0, d_{n+1} = 1$ 19

Figure 2.8. pulse positions of a sample DS-PPM modulated signal 20

Figure 3.1. Optically based UWB system 23

Figure 3.2. FPG based optical UWB system 24

Figure 3.3. FPG frequency response 24

Figure 3.4. Proposed system for single user UWB over FSO communication . 25

Figure 3.5. Comparision of the simulated and theoretical DEP's for weak, moderate and strong turbulence fading conditions 29

Figure 4.1. Proposed system for multiuser communication 30

Figure 4.2. Pulse positions of the first user and an interfering user with 0, min, max time delays. 33

Figure 4.3. Average BER of the TH-PPM UWB system versus user number for a repetition code with $N_s = 1$ 36

Figure 4.4. Average BER of the TH-PPM UWB system versus user number for a repetition code with $N_s = 2$ 36

Figure 4.5. Distribution of multiuser interference with 8 users and no turbulence fading at the output of correlator and gauss distribution with the same variance 39

Figure 4.6. Distribution of multiuser interference with 8 users and weak turbulence fading at the output of correlator and gauss distribution with the same variance 40

Figure 4.7. Distribution of multiuser interference with 8 users and moderate turbulence fading at the output of correlator and gauss distribution with the same variance 41

Figure 4.8. Synchronous multiuser FSO performance with no fading 44

Figure 4.9. Synchronous multiuser FSO performance under weak turbulence . 44

Figure 4.10. Synchronous multiuser FSO performance under weak turbulence when the same channel is used by all users 45

Figure 4.11. Synchronous multiuser FSO performance under moderate turbulence 46

Figure 4.12. Decorrelating Detector performance 46

LIST OF TABLES

Table 2.1. Comparison Between Radio and IM/DD Infrared Systems for Indoor Wireless Communication 6

LIST OF SYMBOLS/ABBREVIATIONS

$c_j^{(k)}$	TH code for kth user at jth frame
d_k	kth bit of the UWB signal
$E[.]$	Expectation function
$G(.)$	Meijer G function
I	Atmospheric turbulence
j	frame number of the UWB signal
$\mathbf{n}$	Noise vector for additive white Gaussian noise
N_h	Max number of TH shift
N_s	Number of monocycles that represents one bit
p	UWB pulse
$p(.)$	Probability density function
P_e	Error probability
$\mathbf{R}$	Covariance matrix of the decorrelating detector
$R(.)$	Correlation function of the UWB receiver
T_f	UWB signal frame period
T_p	PPM Symbol delay
T_s	Symbol duration
T_w	UWB pulse width
$u(.)$	Unit step function
X_{PAM}	Amplitude modulated pulse trains
X_{PPM}	Position modulated pulse trains
X_r	Received signal
X_t	Transmitted signal
v	Correlator at the receiver
α	Gamma-Gamma distribution rate parameter
$\alpha_{i,k}$	Error of delay rounding for kth user
β	Gamma-Gamma distribution rate parameter
η	Photodetector efficiency
γ_p	Signal to Noise Ratio

σ_I^2	Variance of Athmospheric turbulence fading
σ^2	Noise variance
$\tau^{(k)}$	The time delay of the kth user

AWGN	Additive white Gaussian noise
BER	Bit error rate
BS	Base Station
CDMA	Code division multiple access
CS	Central station
DS	Direct sequence
EDFA	Erbium-doped fiber amplifier
FCC	Federal communications commission
FPLD	Fabry-Perot laser diode
FSO	Free space optics
i.i.d	Independent identically distributed
IR	Impulse Radio
LOS	Line of sight
MAI	Multiple access interference
ML	Maximum likelihood
PAM	Pulse amplitude modulation
PD	Photodiode
PDF	Probability density function
PPM	Pulse position modulation
SNR	Signal-to-noise ratio
TF	Tunable Filter
TH	Time Hopping
UWB	Ultrawide-band
WPAN	wireless personal area networks

1. INTRODUCTION

Ultra wideband (UWB) communications is a fast emerging technology that offers new opportunities and expected to have a major impact on the wireless world vision of 4G systems The important characteristics of UWB signals are their huge bandwidth (3.1 to 10.6 GHz, and more recently 57-64 GHz) and their very weak intensity, comparable to the level of parasitic emissions in a typical indoor environment (FCC part 15: -41.3 dBm/MHz). The ultimate target of UWB systems is to utilize broadband unlicensed spectrum (FCC: part 15: 3.1-10.6 GHz) by emitting noise-like signals. The major UWB advantages are potentially low complexity and low power consumption that implies that UWB technology is suitable for broadband services in the mass markets of wireless personal area networks (WPAN). Furthermore, UWB combines the high data rates with capabilities of localization and tracking features, and hence opens the door for many other interesting applications as accurate tracking and location, safety and homeland security. For these reasons, UWB is considered a complementary communication solution within the future 4G systems.

However, the current high data rate UWB systems (e.g. 480 Mbps see [13]) and future evolving multi-gigabit UWB version IEEE802.15.3c at 60GHz are inherently limited to short-ranges of less than 10m. This is simply derived from the constraints on allowed emission levels and fundamental limits of thermal noise and Shannon limits. Larger coverage of high data rate UWB to say 10 10000 meters is most desired for broadband access technology.

One way to extend UWB coverage is to carry UWB signal over optical fibers [1], [5], [7],[8], [14], [15]. Fiber cables offer very high bandwidths that is the basic requirement for ultra short UWB pulses. Fiber cables are nearly immune to background noise and co-channel interference.And it provides nearly nonexistent integration into the fixed wired networks or wireless wide-area infrastructures. Moreover, fiber cables are not effected by multi path fading which is one of the most important problem for UWB RF channels. Finally, generation of UWB pulses on the optical domain requires

cheaper and simpler components with advantages, such as light weight, small size, large tunability and the immunity to electromagnetic interference [7], [14].

On the other hand, recently free space optics gain attraction as an optical approach to the wireless communication for high speed broadband access. Optical signals are carried over atmosphere instead of fiber cables in the FSO systems different than other optical systems. Thus, fiber cable costs are eliminated for the FSO systems which satisfies the main motivation against fiber systems. FSO systems can cost one third to one tenth the price of conventional underground fiber-optic installations [16]. Obviously, FSO can not be compared with fiber systems from the attenuation viewpoint that the free space optical link approach suffers a 41 dB loss over 10km compared to the extremely low loss level of optical fibers that is about 3dB at wavelength $1.55\mu m$. Moreover, under some weather conditions such as heavy fog, the maximum link distance is only at the range of a few hundred meters, regardless of the value of the transmitted power or the size of the receive optics. To overcome this major drawback, the most cost-effective solution is to incorporate an RF back-up. There are several studies to transmit data using RF and FSO channels in parallel [17], [18], [19].

In this thesis, we propose a new concept for converging between the high data rate wireless short-range communications based on UWB technologies and the free space optical access technology. The main idea behind the proposed concept is to enable the transmission of UWB radio signals transparently over optical channels. Since the UWB pulses are carried over optical link very simple optical receivers will be able to convert optical signal into UWB pulses and feed into the UWB RF transmitter. RF UWB communication is best for indoor communication whereas the fiber links are best candidate to carry UWB signals intercity. UWB over FSO fills the gap urban communication up to 10 kilometers with low cost.

Thus, first requirement for the proposed system is that system shall be able to take optical signal as an input or signals can be generated in the optical domain directly. Other requirement is output of the systems shall be converted easily to the RF UWB signal that matches the FCC of US mask. Also system shall provide low bit

error rates at high data rates. Finally, system shall support multiuser access. System architecture, bit error rates for single and multiuser cases are given in the thesis. Also BER simulations are validated with theoretical results for different turbulence regimes and receiver models.

1.1. Thesis Outline

In Chapter 2, we introduce UWB signal model and FSO channel model. This chapter may also be regarded as literature review part. In Chapter 3, an UWB over FSO system is developed using various signal generation methods. Error performance analysis of the proposed system are derived analytically. And simulation results are given for various FSO channel parameters. In Chapter 4, performance of various receiver types are shown for different multiuser communication case. The simulation results are given for FSO links according to the average SNR information provided by the receiver. Finally, the concluding remarks are drawn out in Chapter 5.

2. Free-Space Optical Communications

Over the last two decades, wireless communications have gained enormous popularity. Wireless offers an attractive option for many personal as well as organizational communication needs because of flexibility, cost effectiveness, and mobility. Wireless communication minimizes the cost of cabling and offers flexible installation leading to simpler network infrastructure.

Two transmission techniques for wireless communications have been deployed; Radio Frequency (RF) and wireless optical also called as free space optics (FSO). The well-established industry experience in radio frequency led to quick development of RF-based wireless technologies. The RF wireless systems offer a wide range of coverage and a host of compatible devices. On the other hand, the growing demand of broadband applications and congestion of RF spectrum have fueled interest in the development of the infrared option with much higher data rates compared to RF.

As a channel for medium-range up to 1 km and short-range up to 10 meters, wireless optical radiation offers several significant advantages over radio. optical emitters and detectors capable of highspeed operation at GHz speed are available at low cost. The infrared spectral region offers a virtually unlimited bandwidth that is unregulated worldwide. Infrared and visible light are close together in wavelength, and they exhibit qualitatively similar behavior. Both are absorbed by dark objects, diffusely reflected by light-colored objects, and directionally reflected from shiny surfaces. Both types of light penetrate through glass, but not through walls or other opaque barriers, so that infrared transmissions are confined to the room in which they originate. This signal confinement makes it easy to secure transmissions against casual eavesdropping, and it prevents interference between links operating in different rooms. For the outdoor systems, receiver should be directly align with the incoming signal beam which makes optical links more secure than RF links.

There are also several drawbacks of the wireless optical systems. Because infrared cannot penetrate walls, communication from one room to another requires the installation of infrared access points that are interconnected via a wired backbone. For the outdoor systems any blocking object, such as a bird flying through the optical link between transmitter and receiver may drop communication for short time. In optical environments there exists intense ambient infrared noise, arising from sunlight, incandescent lighting and fluorescent lighting, which induces noise in an infrared receiver. Another problem for the outdoor wireless optical systems is the atmospheric conditions that cause fading and attenuation. In virtually all short-range, optical applications, IM/DD is the only practical transmission technique. The signal-to-noise ratio (SNR) of a direct detection receiver is proportional to the square of the received optical power, implying that IM/DD links can tolerate only a comparatively limited path loss. Often, infrared links must employ relatively high transmit power levels and operate over a relatively limited range. While the transmitter power level can usually be increased without fear of interfering with other users, transmitter power may be limited by concerns of power consumption and eye safety, particularly in portable transmitters. The characteristics of radio and optical wireless links are compared in Table 2.1 [30].

Radio and infrared are complementary transmission media, and different applications favor the use of one medium or the other. Radio is favored in applications where user mobility must be maximized or transmission through walls or over long ranges is required and may be favored when transmitter power consumption must be minimized. Infrared is favored for short-range applications in which per-link bit rate and aggregate system capacity must be maximized, cost must be minimized, international compatibility is required, or receiver signal-processing complexity must be minimized.

Wireless optical systems are used for two main purposes. These are indoor and outdoor systems. An outdoor system which is also called as long distance system usually connects receivers and transmitters that are 100s of meters apart. An outdoor system is mainly used for bridging two different networks. As a result, long distance systems must offer a high bit rate, which conventionally requires the use of high optical power sources such as laser. Accordingly, transmitters and receivers are commonly

Table 2.1. Comparison Between Radio and IM/DD Infrared Systems for Indoor Wireless Communication

Property of Medium	Radio	Wireless optic	Implication for wireless optic
Bandwidth Regulated?	Yes	No	Approval not required.
Passes Through Walls?	Yes	No	Less coverage. More easily secured. Independent links in different rooms.
Multipath Fading?	Yes	No	Simple link design.
Multipath Distortion?	Yes	Yes	
Path Loss	High	High	
Dominant Noise	Other Users	Background Light	Limited range.
Input X(t) Represents	Amplitude	Power	Difficult to operate outdoors.
SNR Proportional to	$\int \lvert X(t)\rvert^2 dt$	$\int \lvert X(t)\rvert^2 dt$	High transmitter power requirement.
Average Power Proportional to	$\int \lvert X(t)\rvert^2 dt$	$\int X(t)dt$	Choose waveform X(t) with high peak-to-average ratio.

mounted on buildings roofs or in safe places where humans cannot interrupt the beams.

2.1. Free-Space Optical Channel Characteristics

It is important to know the characteristic behavior of the FSO channel in order to design good detection algorithms at the receiver. The non-stationary atmospheric processes, divergence (or beam spreading), absorption, scattering, refractive turbulence, and displacement, are the factors that most limit the performance of FSO systems. A brief description of each is given in the following paragraphs.

2.1.1. Divergence

Laser beams diverge on the free space or reflection occurs depending on the receivers reflective index and the angle between receiver lens and received signal's

prorogation axis. Divergence determines how much useful signal energy will be collected at the receive end of a communication link. It also determines how sensitive a link will be to displacement disturbances

2.1.2. Absorption

Molecules of some gases in the atmosphere absorb laser light energy; primarily water vapor, Carbon Dioxide (CO_2), and Methane, Natural Gas (CH_4). The presence of these gases along a path changes unpredictably with the weather over time. Thus their effect on the availability of the link is also unpredictable. Another way of stating this is that different spectrum windows of transmission open up at different times, but to take advantage of these, the transmitter would have to be able to switch (or return) to different wavelengths in a sort of wavelength diversity technique.

2.1.3. Scattering

Another cause of light wave attenuation in the atmosphere is scattering from aerosols and particles. The actual mechanism is known as Mie scatter in which aerosols and particles comprising fog, clouds, and dust, roughly the same size as the lights wavelength, deflect the light from its original direction. Some scattered wavelets travel a longer path to the receiver, arriving out of phase with the direct (unscattered) ray. Thus destructive interference may occur which causes attenuation.

Divergence, absorption and scattering effects can be shown in one equation which is called as free-space optic link equation

$$P_r = P_t \frac{A_r}{(D \times R)^2} \exp(-\alpha \times R) \tag{2.1}$$

where P_r is received power at the photo-detector, P_t is transmitted power from the light source, A_r is the area of photo-detector, D is the divergence of laser beam, R is the distance between transmitter and receiver and α is the attenuation coefficient. Here, $P_t \frac{A_r}{(D \times R)^2}$ part is called as geometric loss which is caused by divergence and

$\exp(-\alpha \times R)$ called as attenuation loss which is caused by absorption and scattering. α factor depends on atmospheric conditions and can be found by experiments.

2.1.4. Turbulence

In the laminar region light refraction is predictable and constant, whereas in the turbulent region it changes from point to point, and from instant to instant. Small temperature fluctuations in regions of turbulence along a path cause changes in the index of refraction. One effect of the varying refraction is scintillation which is caused by random fluctuations in the amplitude of the light. Another effect is random fluctuations in the phases of the lights constituent wavelengths. Refractive turbulence is common on rooftops where heating of the surface during daylight hours leads to heat radiation throughout the day.

2.1.5. Displacement

For an FSO link, alignment is necessary to ensure that the transmit beam divergence angle matches up with the field of view of the receive telescope. However, since FSO beams are quite narrow, misalignment due to building twist and sway as well as refractive turbulence can interrupt the communication link. One method of combating displacement is to defocus the beam so that a certain amount of displacement is possible without breaking the link. Another method is to design the FSO head with a spatial array of multiple beams so that at least one is received when the others are displaced. The latter technique circumvents the problem of displacement without sacrificing the intensity of the beam.

2.2. Atmospheric Turbulence

Atmospheric-induced scintillation is a major impairment of FSO communications systems. Because of the complexity associated with phase or frequency modulation, current free-space optical communication systems typically use intensity modulation with direct detection (IM/DD). Atmospheric turbulence can degrade the performance

of free-space optical links, particularly over ranges of the order of 1 km or longer. Inhomogeneities in the temperature and pressure of the atmosphere lead to variations of the refractive index along the transmission path. These index inhomogeneities can deteriorate the quality of the received image and can cause fluctuations in both the intensity and the phase of the received signal. These fluctuations can lead to an increase in the link error probability, limiting the performance of communication systems. Turbulence is divided in three regions depending on the fading severity. First one is weak turbulence which can be experienced in the open air conditions. Second one is moderate turbulence refer to the conditions where scintillation indexes exceeding 0.75 Final region is strong turbulence where the scintillation indexes equals to 1. In general, a scintillation index is a complicated function of the beam parameters, propagation distance, heights of the transmitter and receiver, and the fluctuations in the index of refraction. In fact, the main source of scintillation is due to fluctuations (due to temperature variations) in the index of refraction, which is commonly known as optical turbulence. In all scenarios, the impact of turbulence on the complex field may be modeled as a multiplicative, complex exponential term.

2.2.1. Weak Turbulence

For this case, the probability density function (PDF) of the log-normal distributed received intensity is given by

$$f_I(I) = \frac{1}{2I\sqrt{2\pi\sigma_x^2}} \exp\left(-\frac{(\ln(I/I_0))^2}{8\sigma_x^2}\right),\ I \geq 0. \tag{2.2}$$

The scintillation index is the normalized variance of fading intensity and it is defined as $\sigma_{SI}^2 = E[I^2]/E[I]^2 - 1 = e^{\sigma_x^2} - 1$. For instance, the log-normal distribution for the light intensity in (2.2) represents the condition where the amplitude fluctuations are weak and single scatters dominate the channel, which is valid for $0 \leq \sigma_{SI}^2 \leq 0.75$.

For propagation distances less than a few kilometers, variations of the log-amplitude are typically much smaller than variations of the phase. Over longer propagation distances, where turbulence becomes more severe, the variation of the log-amplitude can

become comparable to that of the phase. Based on the proposed system and assuming weak turbulence, we can obtain the approximate analytic expression for the covariance of the log-amplitude fluctuation X of plane wave [27] as

$$\sigma_X^2 = 0.56 \left(\frac{2\pi}{\lambda}\right)^{7/6} \int_0^L C_n^2(x)(L-x)^{5/6} dx \tag{2.3}$$

where λ is wavelength, L is propagation distance and C_n is the wavenumber spectrum structure parameter, which is altitude-dependent [28]

$$C_n^2(z) = K_0 z^{-1/3} exp\left(\frac{-z}{z_0}\right) \tag{2.4}$$

where K_0 is parameter describing the strength of the turbulence and z_0 is effective height of the turbulent atmosphere. For atmospheric channels near the ground ($z < 18.5m$), C_n^2 can vary from $10^{-13}m^{-2/3}$ for strong turbulence $10^{-17}m^{-2/3}$ to for weak turbulence, with $10^{-15}m^{-2/3}$ often called as a typical average value [29].

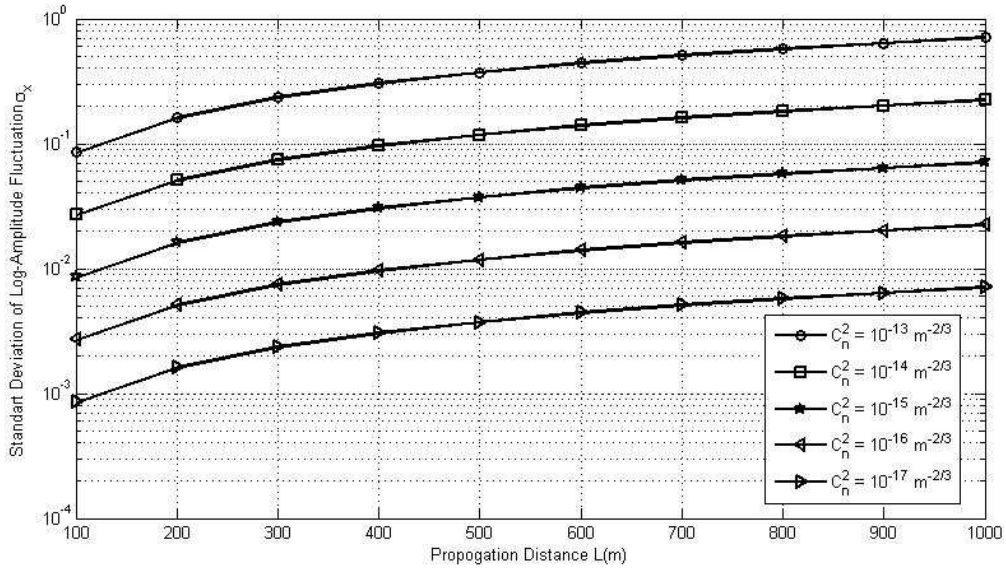


Figure 2.1. Standard deviation of the log-amplitude fluctuation versus propagation distance for a plane wave

Fig. 2.1 shows the standard deviation of the log-amplitude fluctuation σ_X for a plane wave as a function of the propagation distance L. Regarding the proposed system, L is chosen between 100 and 1000, carrier wavelength λ is chosen as 1550nm

and $C_n^2(z)$ is assumed to be constant.

2.2.2. Moderate Turbulence

Under moderate turbulence conditions, both the small and large scatterers are effective and the intensity fluctuations are modelled by the Gamma-Gamma distribution described by the PDF

$$f_I(I;\alpha,\beta) = \frac{2(\alpha\beta)^{\frac{\alpha+\beta}{2}}}{\Gamma(\alpha)\,\Gamma(\beta)} I^{\frac{\alpha+\beta}{2}-1} K_{\alpha-\beta}\left(2\sqrt{\alpha\beta I}\right) \tag{2.5}$$

where $\Gamma(\cdot)$ and $K_n(\cdot)$ are the Gamma function and the nth-order modified Bessel function of the second kind, respectively. Small and large scale scattering effects that are represented by α and β, respectively in (3.13) are related to the atmospheric conditions by

$$\begin{aligned} \alpha &= \left[\exp\left(\frac{0.49\chi^2}{(1+0.65d^2+1.1\chi^{12/5})^{7/6}}\right)-1\right]^{-1} \\ \beta &= \left[\exp\left(\frac{0.51\chi^2\left(1+0.69\chi^{12/5}\right)^{-5/6}}{(1+0.9d^2+0.62d^2\chi^{12/5})^{5/6}}\right)-1\right]^{-1} \end{aligned} \tag{2.6}$$

where $\chi^2 = 0.5C_n^2k^{7/6}L^{11/6}$ is the Rytov variance for a plane wave and the parameters where C_n^2 is an altitude-dependent parameter and in literature often referred as refractive-index structure parameter, $k = 2\pi/\lambda$ is the optical wave number, where λ is the wavelength of the transmitted pulse and L is the link distance [25]. These parameters are related to the scintillation index by $\sigma_{SI}^2 = \alpha^{-1} + \beta^{-1} + (\alpha\beta)^{-1}$ and moderate turbulence regime is often characterized as the one with $0.75 \leq \sigma_{SI}^2 < 1$.

2.2.3. Strong Turbulence

Finally, the strong turbulence conditions are modeled as one-sided negative exponential distribution given by

$$f(I) = \frac{1}{\overline{I}} \exp\left(-\frac{I}{\overline{I}}\right), \; I \geq 0 \tag{2.7}$$

where $\overline{I}$ denotes the mean light intensity. This case represents the condition with many non-dominating scatterers. This saturation regime corresponds to scintillation index $\sigma_{SI}^2 \geq 1$.

2.3. Ultra Wideband Signal

UWB usually refers to impulse based waveforms that can be used with different modulation schemes. The transmitted signal consists of a train of very narrow pulses at baseband, normally on the order of a nanosecond. Each transmitted pulse is referred to as a monocycle. The information can be carried by the position or amplitude of the pulses. In general, narrower pulses in the time domain correspond to electromagnetic radiation of wider spectrum in the frequency domain. Thus, the baseband train of nanosecond impulses can have a frequency spectrum spanning from zero to several GHz, resulting in the so called UWB transmission. The unique advantages of the UWB spectral occupancy are enhanced capability to penetrate through obstacles, ultra high precision ranging at the centimeter level, potential for very high data rates along with a commensurate increase in user capacity and potentially small size and processing power. Despite these attractive features, interest in UWB devices prior to 2001 was primarily limited to radar systems, mainly for military applications.

In 2002, FCC released a spectral mask allowing (even commercial) operation of UWB radios at the noise floor fig. 2.2 over an enormous bandwidth (up to 7.5 GHz). Regarding the wireless communications in particular, the FCC regulated power density of the UWB signal in a narrow frequency band is very small (below -41.3 dBm), compared to other modulation schemas. Thus, UWB signals are threatened

as a small additive noise by other narrowband systems such as the global positioning system (GPS) and the IEEE 802.11 wireless local area networks (WLANs) that coexist in the 3.6-10.1 GHz band. Although UWB signals can propagate greater distances at higher power levels, current FCC regulations enable high-rate (above 110 MB/s) data transmissions over a short range (10-15 m) at very low power.

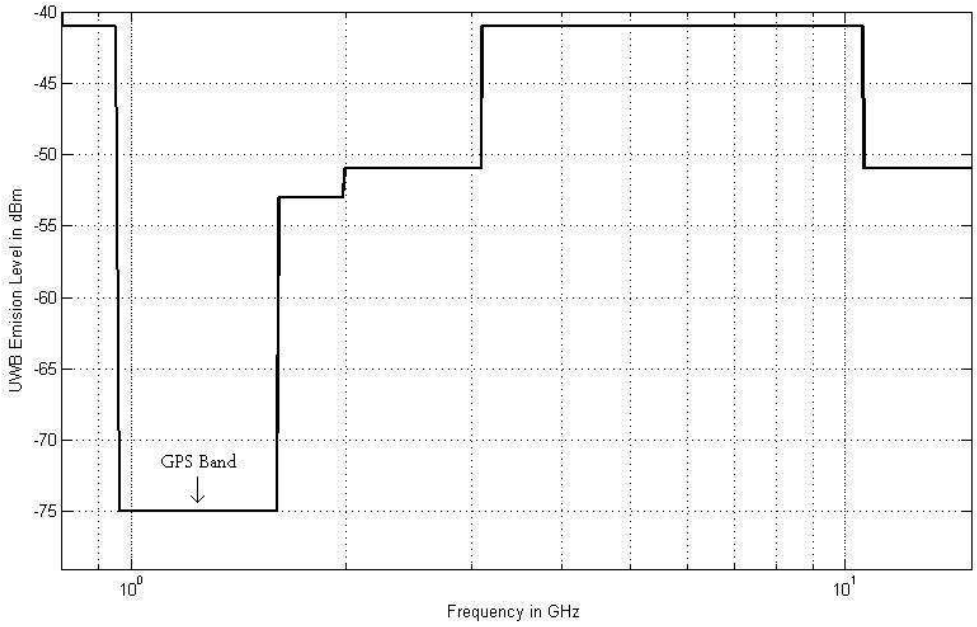


Figure 2.2. FCC spectral mask for UWB communication

UWB communication is used for short-range (generally within 10-20 m) wireless personal area networks (WPANs). UWB signal provides high-quality real-time video and audio distribution, file exchange among storage systems, and cable replacement for home entertainment systems, portable consumer electronic and communication devices. Another application is sensor networks that consist of a large number of nodes spread across a geographical area. Key requirements for sensor networks operating in challenging environments include low cost, low power, and multifunctionality. High data-rate UWB communication systems are well motivated for gathering and disseminating or exchanging a vast quantity of sensory data in a timely manner. Typically, energy is more limited in sensor networks than in WPANs because of the nature of the sensing devices and the difficulty in recharging their batteries.

2.3.1. Monocycle Waveforms

UWB systems are depends on the ultra short duration impulsive signals. Thus impulse characteristics is directly effects the system behavior. There are several considerations when concerning to design an UWB signal. First and the most important restriction is the regulation of US of FCC. FCC defines a spectrum mask for UWB signals to decrease the interference of UWB to the other communication networks like GSM. Simple transmitter design and coexistence of other spread spectrum systems are also main criteria. Typical pulse waveforms used in research include rectangular, Gaussian, Gaussian doublet, and Rayleigh monocycles [6].

A rectangular monocycle with width T_w and unity energy can be represented by $\sqrt{\frac{1}{T_w}}\left[U(t) - U(t - T_w)\right]$ where $U(.)$ denotes the unit step function. The rectangular pulse has a large DC component, which is not a desired property. Even so, the rectangular monocycle has often been used in academic research because of its simplicity. A generic Gaussian pulse is given by

$$p_g(t) = \frac{1}{\sqrt{2\pi}\sigma} exp\left[-\frac{1}{2}\left(\frac{t-\mu}{\sigma}\right)^2\right] \tag{2.8}$$

where μ defines the center of the pulse and σ determines the width of the pulse. Some popular monocycles are derived from the Gaussian pulse. The Gaussian monocycle is the second derivative of a Gaussian pulse, and is given by

$$p_G(t) = A_G\left[1 - \left(\frac{t-\mu}{\sigma}\right)^2\right] exp\left[-\frac{1}{2}\left(\frac{t-\mu}{\sigma}\right)^2\right] \tag{2.9}$$

where the parameter σ determines the monocycle width T_p. The effective time duration of the waveform that contains 99.99% of the total monocycle energy is $T_p = 7\sigma$ centered at $\mu = 3.5\sigma$. The factor A_G is introduced so that the total energy of the monocycle is normalized to unity, i.e $\int p_G^2(t)dt = 1$.

The Gaussian doublet is a bipolar signal, consisting of two amplitude reversed

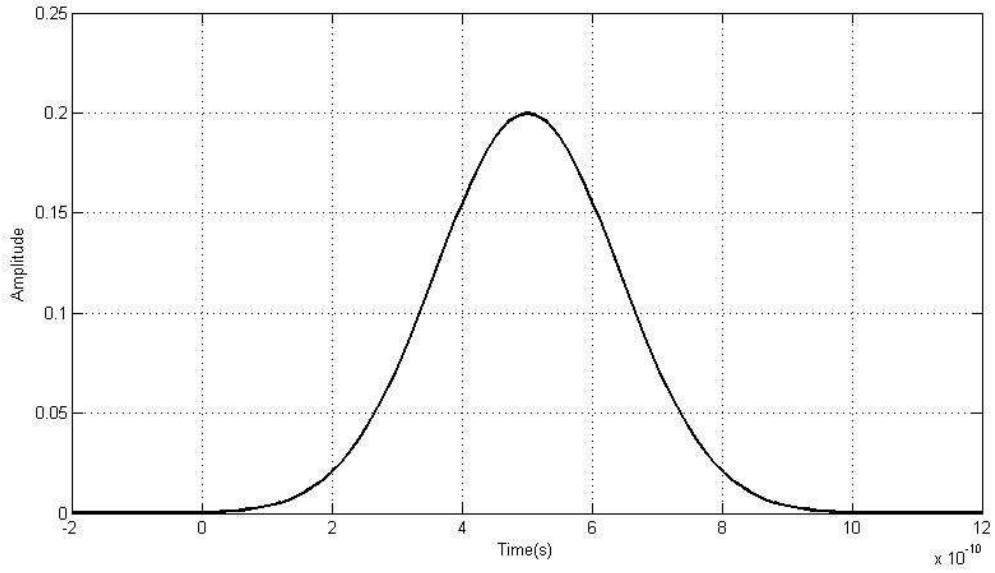


Figure 2.3. Gaussian pulse

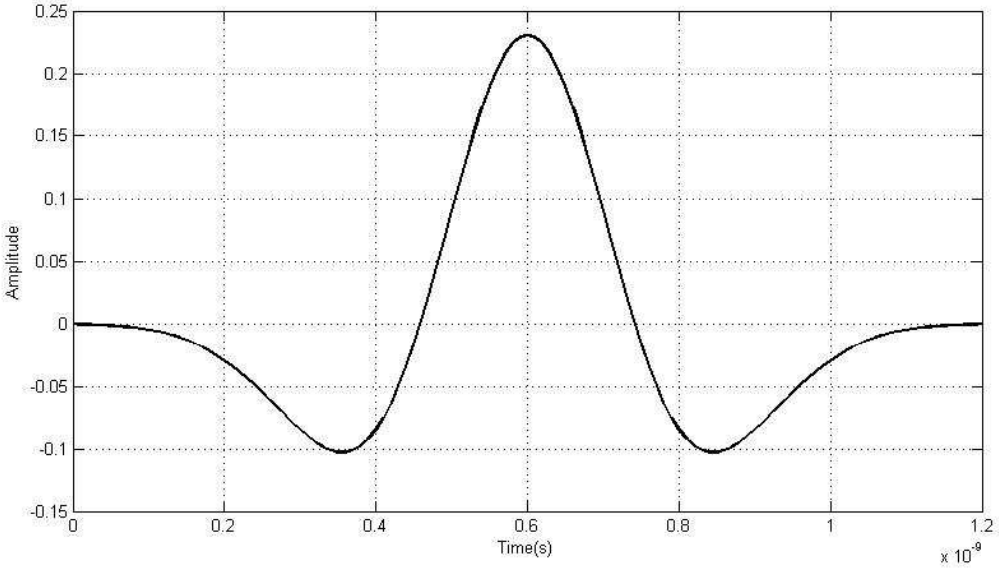


Figure 2.4. Gaussian monocycle

Gaussian pulses with a time gap of T_w between the two pulses. The mathematical expression for the monocycle is

$$p_{GD}(t) = A_{GD}\left\{exp\left[-\frac{1}{2}\left(\frac{t-\mu}{\sigma}\right)^2\right] - exp\left[-\frac{1}{2}\left(\frac{t-\mu-T_w}{\sigma}\right)^2\right]\right\}. \tag{2.10}$$

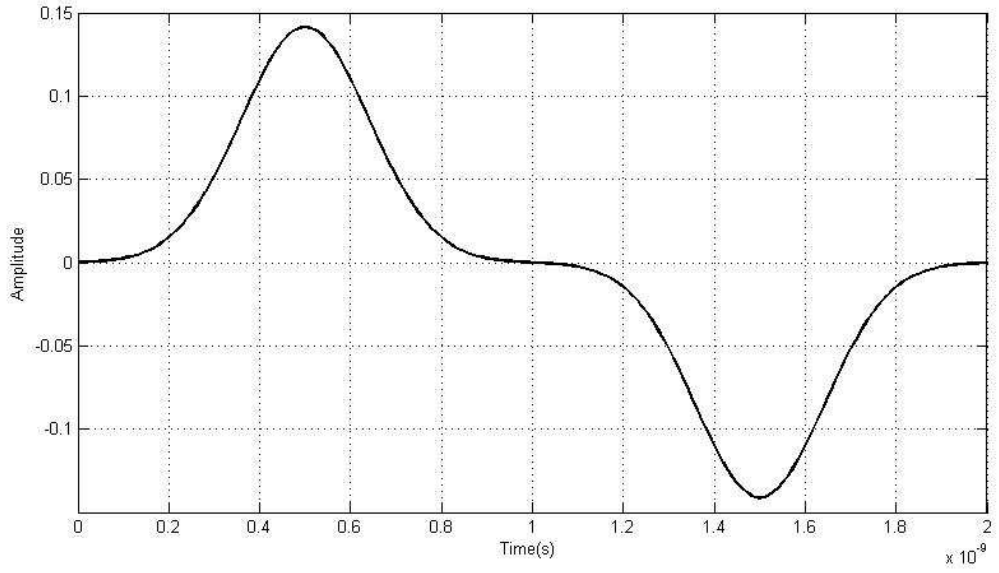


Figure 2.5. Gaussian doublet

2.3.2. Modulation Schemas

Mostly used modulation methods for UWB system are pulse position modulation (PPM) and pulse amplitude modulation (PAM). Also various modulation options for UWB systems are discussed in terms of their spectral characteristics and hardware complexities in[20] for TH modulation and in [22] for TH, DS and OOC modulations. In PPM modulation every symbol represented with a pulse delay and in PAM symbols are represented by amplitude of the pulses. Notice that phase modulation is not applicable to UWB systems due to it's carrier-less nature. A PAM signals can be shown as

$$X_{PAM}(t) = \sum_{k=0}^{\infty} a_k p(t - kT_f) \tag{2.11}$$

where T_f is the frame period, $p(t)$ is UWB pulse and a_k is the PAM code which depends on data symbol. For a binary system

$$a_k = \begin{cases} -1 & \text{if } d_k = 0, \\ 1 & \text{if } d_k = 1 \end{cases} \tag{2.12}$$

PPM is based on the principle of encoding information with two or more positions in time, referred to the nominal pulse position, as shown in Figure 2.6. A pulse transmitted at the nominal position represents a 0, and a pulse transmitted after the nominal position represents a 1. The picture shows a two-position modulation,where one bit is encoded in one impulse.

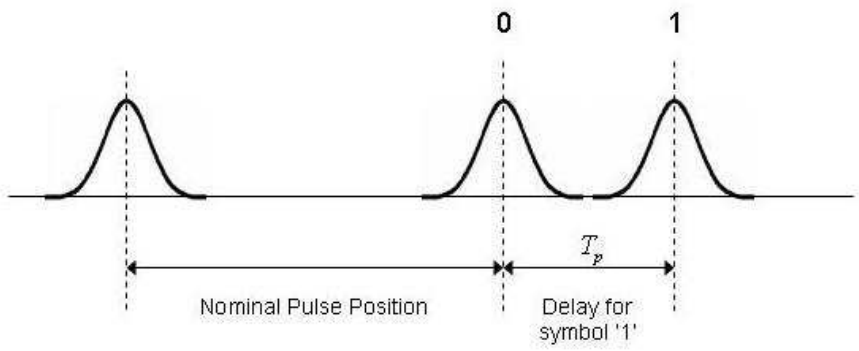


Figure 2.6. Pulse Position Modulation Structure

The PPM equation can be written as

$$X_{PPM}(t) = \sum_{k=0}^{\infty} p(t - kT_f - d_k T_p) \tag{2.13}$$

where $d_k \in \{0, 1\}$ is k data bit and T_p is time delay for symbol '1'.

Additional positions can be used to provide more bits per symbol. The time delay between positions is typically a fraction of a nanosecond, while the time between nominal positions is typically much longer to avoid interference between impulses.

In the proposed system, direct detection is used that converts intensity of the optical signals into the electrical signal. Negative components will be lost at the receiver side that makes PPM is the only modulation schema that provides requirements of the proposed system. Thus, PPM modulation will be used in system analysis.

2.3.3. Multiple-Access Techniques

There are two main multiple access modulation types for UWM systems which are time hopping (TH) and direct sequence (DS) [21] .

For the TH scheme, one bit is represented by N_s frames. The equation below shows uth user's signal with PPM modulation

$$X^{(u)}_{TH_PPM}(t) = \sqrt{\frac{1}{N_s}} \sum_{k=0}^{\infty} \sum_{j=0}^{N_s} p(t - jT_f - d^{(u)}_k T_p) \tag{2.14}$$

Then distinct TH codes $c^{(k)}_j$ are assigned to each user to add extra delay to the mono-cycles in a frame in order to avoid catastrophic collisions in multiple access.

$$X^{(u)}_{TH_PPM}(t) = \sqrt{\frac{1}{N_s}} \sum_{k=0}^{\infty} \sum_{j=0}^{N_s} p(t - jT_f - c^{(u)}_j T_c - d^{(u)}_k T_p) \tag{2.15}$$

where T_c is the delay applied by TH codes. Fig. 2.7 shows the structure of TH-PPM system for two consecutive frames. The transmission data rate R_s for the TH system can be found as $1/(N_s T_f)$ in bps.

In a synchronized network, an orthogonal TH sequence that satisfies $c^{(k)}_j \neq c^{(k')}_j$ for all j's and for any two users $k \neq k'$ can be adopted to minimize interference between the users. The performance of synchronous multiple access systems using various TH sequences such as the Gold sequence and a simulated annealing code has been studied in the literature. For asynchronous system, the choice of orthogonal TH sequence does not guarantee collision-free transmission.

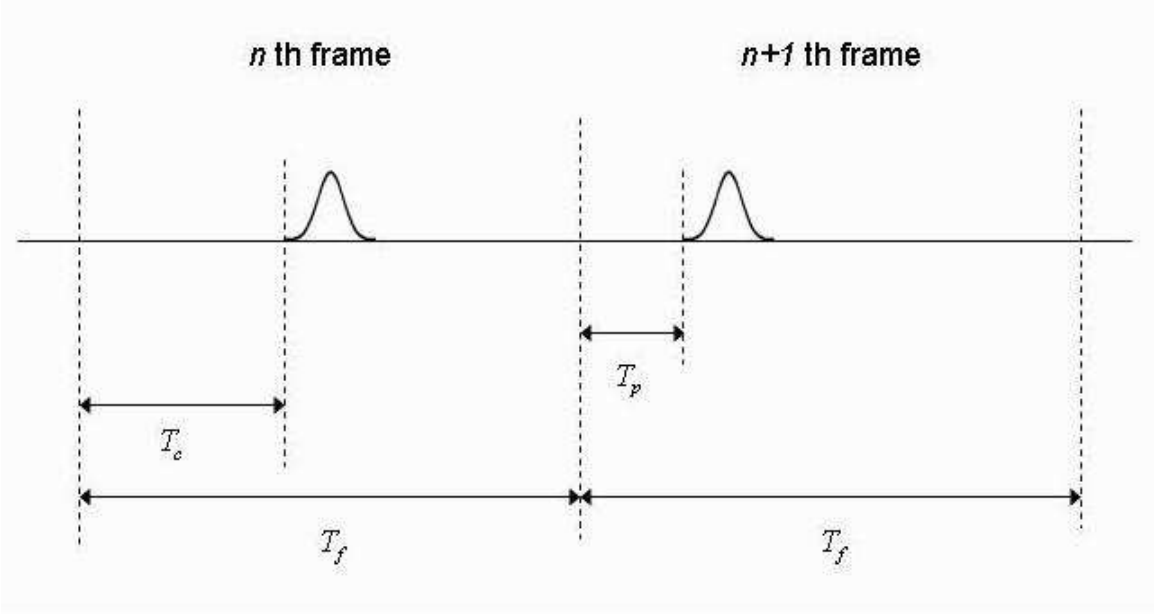


Figure 2.7. Pulse position for two consecutive frames of TH-PPM modulation with $c_n = 1, c_{n+1} = 0$ and $d_n = 0, d_{n+1} = 1$

Direct sequence UWB employs a train of high duty cycle pulses whose polarities follow pseudo-random code sequences. Specifically, each user in the system is assigned a pseudo-random sequence that controls pseudorandom inversions of the UWB pulse train.

In a DS-UWB system with PPM modulation, the binary symbol d_k to be transmitted over the kth frame is spread by a sequence of multiple monocycles $\{A_j^{(u)} p(t - kT_f - jT_c)\}_{j=0}^{N_h-1}$, whose polarities are determined by the spreading sequence $A_j^{(u)}{}_{j=0}^{N_h-1}$. Such a spreading sequence is assigned uniquely to each user in a multiple access user in order to allow multiple transmissions with little interference. Similar to the TH system an orthagonal spreading sequence such as a Gold sequence or Hadamard-Walsh code can be selected to mitigate multiple access interference in a synchronous network.

The DS-PPM signal transmitted can be described as

$$X_{DS_PPM}^{(u)}(t) = \frac{1}{\sqrt{N_h}} \sum_{k=-\infty}^{\infty} \sum_{j=0}^{N_h-1} A_j^{(u)} p(t - kT_f - jT_c - d_k^{(u)} T_p) \qquad (2.16)$$

where the sequence $\{A_j^{(u)}\}_j = 0^{N_h-1} \in \{-1, 1\}$ represents the pseudorandom code or spreading sequence. The factor $1/\sqrt{N_h}$ is introduced such that the sequences of N_h monocycles has unit energy. An example of a DS-PPM modulated UWB signal for data sequence $\{0, 1, 1\}$ with DS code $\{1, -1, 1, 1\}$ is shown in fig. 2.8.

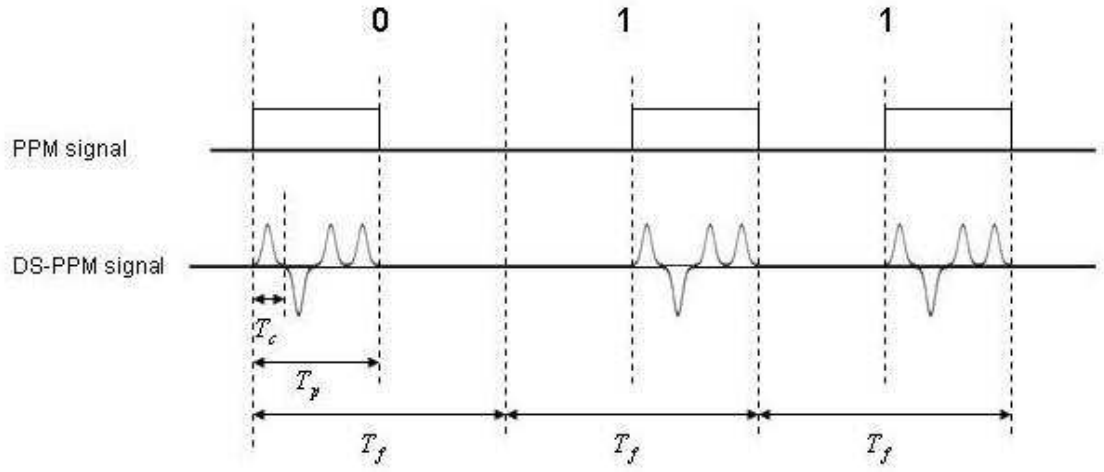


Figure 2.8. pulse positions of a sample DS-PPM modulated signal

DS codes with negative polarization introduces negative pulses to the channel which is not usable for FSO channels. Optical Orthogonal Codes (OOC) are families of binary sequences typically employed to provide multiuser capabilities to "positive" systems (i.e., systems in which the transmitted waveforms can not be summed to obtain zero) such as optic links. These codes are characterized by four parameters $(F, K, \lambda_a, \lambda_c)$ that symbolize respectively the code length, the number of "1" in the code words, and the maximum (out of phase) autocorrelation and cross correlation values. In the proposed system, TH-PPM modulation is used with pseudorandom TH codes.

3. UWB over FSO

In this chapter, we present the performance of UWB over FSO channels for the three fading type as following:

- Log-normal,
- Gamma-gamma,
- Negative exponential.

In the next section, optical generation methods will be presented which is required to carry UWB signal over optical carrier. Then at the channel, atmospheric turbulence effects will be applied to the signal depending on the turbulence regime. At the receiver, single user matched filter will be used to detect and demodulate the data. Finally the error performances are presented with theoretical analysis and simulation results.

3.1. Generation methods

Generation methods of the optical signals can be divided into 2 main categories which are all optical and electro-optical conversion. During the few recent years, researchers have proposed several approaches for the optical generation of Ultra-wideband signals generation which are Chromatic Dispersion based approach, FBG-based Approach, Optical impulse radio (IR) system, Electro-optical intensity modulator based method, Method based on XPM in an SOA, Optical FSK based method, Spectral shaping and dispersion-induced frequency to time conversion based technique [7]. Optical impulse radio will be used in the proposed system due to it's simplicity. Also optical impulse radio method does not use chromatic dispersion property of the fiber cables which is not applicable for the proposed system.

3.1.1. Optical impulse radio (IR) system

One of the most attractive impulse technologies is the carrier- free modulation scheme which does not use the complicated frequency mixer, intermediate frequency, and filter circuits, which greatly reduces the cost. Moreover, it has good pass-through performance due to the base-band transmission and much more suitable for indoor wireless communication. In general, the pulsed wireless communications use only a few complex electronic circuits and radio frequency (RF) components to generate pulse train signals.

Fig. 3.1 shows a basic optical impulse radio system to generate optical impulse radio signal and transmits from central station to base station. Fabry-Perot laser diode (FPLD) modulates laser carrier with input RF signal. FPLD output pass trough an optical tunable filter (TF) in order to obtain a carrier with wider wavelength band. Then, Erbium-doped fiber amplifier is used to amplify the signal before feeding into the free space channel.[8] At the base station a photodiode (PD) converts optical pulses into the electrical form. PD is used for direct detection of the optical signals which detects the energy of the signal. Thus, negative components are not recognized by the receiver and restricts the transmitter using only positive signals. As discussed n the section 2.3.1, all derivatives of the gaussian pulse have negative components and only gaussian pulse itself has only positive components. As a result, a gaussian pulse is used on FSO channel by using a gaussian pulse signal at the input of FPLD. On the other hand, at least first derivate of the gaussian pulse is required to be compliant FCC of US on the RF channel. In order to be compliant with FCC, a microwave differentiator is used to convert PD output into a gaussian monocycle. Differentiator output is fed to the UWB antenna.

3.1.2. FBG-based Approach

Another approach is to use optical differentiator to generate gaussian monocycles proposed by [14]. As seen in the fig. 3.2 optical carrier is phase modulated using a gaussian pulse.The electrical field of the phase modulated light wave can be expressed

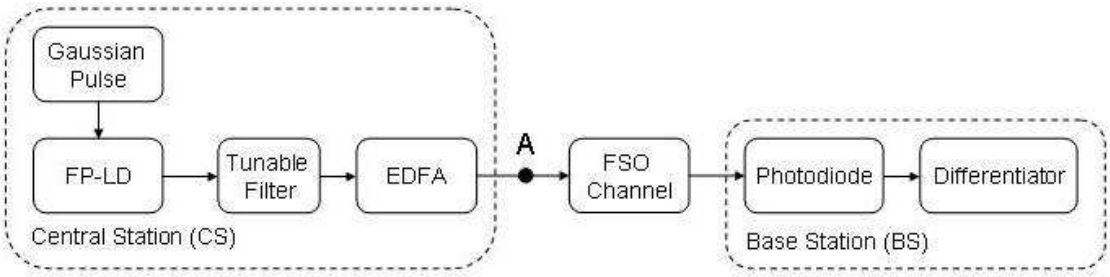


Figure 3.1. Optically based UWB system

as

$$A(t) = exp[j\omega_c t + j\beta_{PM} p(t)], \tag{3.1}$$

where β_{PM} is the phase modulation index, ω_c is the angular frequency of the optical carrier and $p(t)$ is gaussian pulse. The phase modulated optical signal is then fed into an optical frequency discriminator. A frequency discriminator is simply an optical filter having frequency response with two opposite linear slopes as shown in figure 3.3. At the output of the frequency discriminator first order derivative of the gaussian pulse is obtained as

$$A_{out}(t) = [K(\omega_c - \omega_0) + K\beta_{PM} s'(t)]A(t) \tag{3.2}$$

where $s'(t)$ is the first order derivative of $s(t)$. After passing through FSO channel optical signal intensity is converted to the photocurrent via photodetector given by

$$i_{PD}(t) = K^2(\omega_c - \omega_0)^2 + K^2\beta_{PM}^2[s'(t)]^2 + 2K^2(\omega_c - \omega_0)\beta_{PM} s'(t). \tag{3.3}$$

3.2. Error performance

Optical impulse radio generation method with PPM pulse modulation is used for the proposed transmitter. As defined in the previous section a simple gaussian pulse is used to carry bits in order to satisfy positive signal restriction. Signal propagates

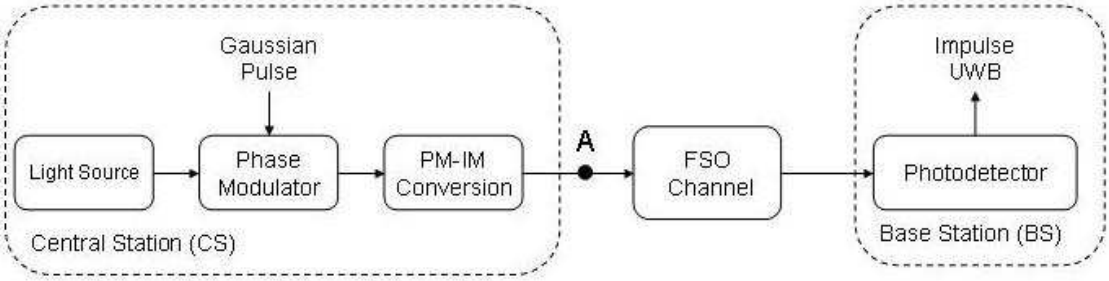


Figure 3.2. FPG based optical UWB system

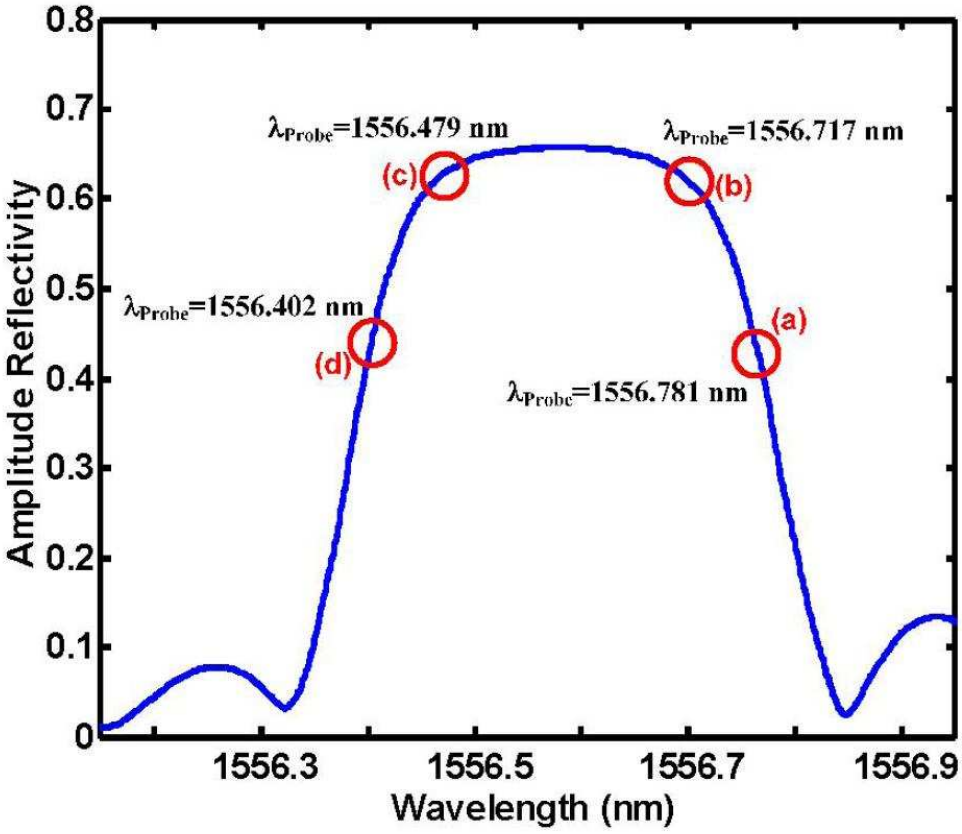


Figure 3.3. FPG frequency response

over free space channel between transmitter and receiver. Channel effects are assumed as background noise and atmospheric turbulence. At the receiver an optical detector converts optical signal into electrical form via direct detection (DD) method. Fig. **??** shows the final system.

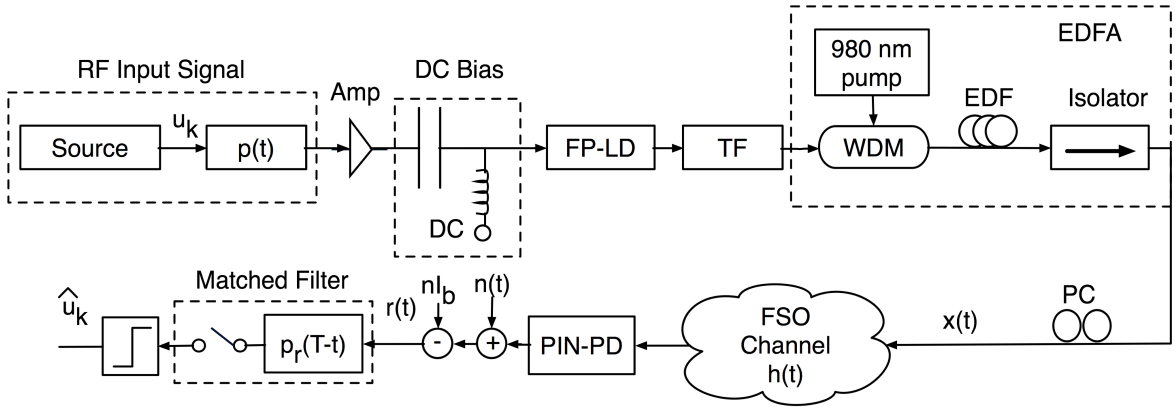


Figure 3.4. Proposed system for single user UWB over FSO communication

A synchronous matched filter with zero threshold detector is used to retrieve the transmitted signal.The transmitted signal can be shown as

$$x_{tFSO}(t) = \sqrt{E_p} \sum_{j=0}^{N_s-1} p(t - jT_f - c_j T_c - d_{[\frac{j}{N_s}]} T_p) \tag{3.4}$$

where E_p is the transmitted pulse energy. After the effects of background noise and atmospheric turbulence fading, received signal is written as

$$x_{rFSO}(t) = \eta I \sqrt{E_p} \sum_{j=0}^{N_s-1} p(t - jT_f - c_j T_c - d_n T_p) + n_b(t). \tag{3.5}$$

At the receiver end, the signal is passed through a matched filter that uses a signal designed for PPM modulation to generate $+1$ for bit 0 and -1 for bit 1 which can be shown as,

$$v(t) = p(t) - p(t - T_p). \tag{3.6}$$

Correlator output is sampled in every frame period and summation of N_s frames fed to the zero threshold detector, since a bit is represented by N_s frames. The signal computed for nth bit at the input of the zero threshold detector is,

$$\begin{aligned} y(nT_d) &= \sum_{j'=nN_s}^{(n+1)N_s} \int_{-\infty}^{\infty} x_{rFSO}(t) v(t - j'T_f - j'T_c) dt \\ &= \sum_{j'=nN_s}^{(n+1)N_s} \int_{-\infty}^{\infty} \eta I \sqrt{E_p} \sum_{j=0}^{N_s-1} p(t - jT_f - c_j T_c - d_{[\frac{j}{N_s}]} T_p) v(t - j'T_f - j'T_c) dt \\ &+ \int_{-\infty}^{\infty} n_b(t) v(t - jT_f - jT_c) dt. \end{aligned} \tag{3.7}$$

Since $\int_{-\infty}^{\infty} p(t - jT_f - c_j T_c - d_{[\frac{j}{N_s}]} T_p) v(t - j'T_f - j'T_c) dt = 0$ for $j \neq j'$ threshold input can be rewritten as

$$\begin{aligned} y(nT_d) &= \sum_{j=nN_s}^{(n+1)N_s} \int_{-\infty}^{\infty} \eta I \sqrt{E_p} p(t - jT_f - c_j T_c - d_{[\frac{j}{N_s}]} T_p) v(t - jT_f - jT_c) dt \\ &+ \int_{-\infty}^{\infty} n_b(t) v(t - jT_f - jT_c) dt \\ &= \pm \eta I N_s \sqrt{E_p} + n_n. \end{aligned} \tag{3.8}$$

So the error probability as a function of the turbulence fading at the output of the zero threshold detector is [23]

$$P_e(I) = Q\left(\sqrt{\frac{(\eta I N_s)^2 E_p}{N_s N_0}}\right) = Q\left(\sqrt{(\eta I)^2 N_s \gamma_p}\right) \tag{3.9}$$

where $\gamma_p = \frac{E_p}{N_0}$ is the signal to noise ratio and the average error probability can be calculated by taking expectation over fading,

$$P_e = E[P_e(I)] = \int_0^{\infty} P_e(I) f_I(I) dI. \tag{3.10}$$

3.2.1. Error performance under weak turbulence

Using Eq. 2.2 and Eq. 3.10 average bit error probability under weak turbulence can be calculated as

$$P_e = \frac{1}{2}\int_0^\infty erfc\left(\sqrt{\frac{(\eta I)^2 N_s \gamma_p}{2}}\right)\frac{1}{2I\sqrt{2\pi\sigma_x^2}}\exp\left(-\frac{(\ln(I/I_0))^2}{8\sigma_x^2}\right)dI \tag{3.11}$$

and closed form of the integral can be found using Gauss-Hermite expansion

$$P_e = \frac{1}{2\pi}\sum_{i=1}^{n}\omega_i erfc\left(\sqrt{\frac{N_s\gamma_p(\eta I_0 e^{y_i\sqrt{8\sigma_x^2}})}{2}}\right). \tag{3.12}$$

3.2.2. Error performance under moderate turbulence

Using Eq. 3.13 and Eq. 3.10 average bit error probability under moderate turbulence can be calculated as

$$P_e = \frac{1}{2}\int_0^\infty erfc\left(\sqrt{\frac{(\eta I)^2 N_s \gamma_p}{2}}\right)\times\frac{2(\alpha\beta)^{\frac{\alpha+\beta}{2}}}{\Gamma(\alpha)\Gamma(\beta)}I^{\frac{\alpha+\beta}{2}-1}K_{\alpha-\beta}\left(2\sqrt{\alpha\beta I}\right) \tag{3.13}$$

and closed form can be found by representing $erfc()$ and $K_v()$ functions as a meijer G function [26]

$$erfc(\sqrt{x}) = \frac{1}{\sqrt{\pi}}G_{1,2}^{2,0}\left[x\middle|\begin{matrix}1\\0,\frac{1}{2}\end{matrix}\right], \tag{3.14}$$

$$K_v(x) = \frac{1}{2}G_{0,2}^{2,0}\left[\frac{x^2}{4}\middle|\begin{matrix}-\\\frac{v}{2},-\frac{v}{2}\end{matrix}\right] \tag{3.15}$$

and using Eq. 07.34.21.0011.01 of [26] in order to product two meijer G functions , equation 3.13 results in a closed-form expression such that

$$P_e = \frac{2^{\alpha+\beta-3}}{\sqrt{\pi^3}\Gamma(\alpha)\Gamma(\beta)} \times G_{5,2}^{2,4}\left[\frac{8\eta^2 N_s\gamma_p}{\alpha^2\beta^2}\middle| \begin{matrix} \frac{1-\alpha}{2}, \frac{2-\alpha}{2}, \frac{1-\beta}{2}, \frac{2-\beta}{2}, 1 \\ 0, \frac{1}{2} \end{matrix}\right]. \tag{3.16}$$

3.2.3. Error performance under strong turbulence

Using Eq. 2.7 and Eq. 3.10 average bit error probability under moderate turbulence can be calculated as

$$\begin{aligned} P_e &= \frac{1}{2}\int_0^\infty erfc\left(\sqrt{\frac{(\eta I)^2 N_s\gamma_p}{2}}\right)\frac{1}{I}exp\left(-\frac{1}{I}\right)dI \\ &= \frac{1}{2}\left[1 - erfc\left(\frac{1}{\eta I\sqrt{2N_s\gamma_p}}\right)exp\left(\frac{1}{(\eta I)^2 2N_s\gamma_p}\right)\right]. \end{aligned} \tag{3.17}$$

3.3. Simulation Results

In this section, error performance of the proposed system is simulated and results are compared with theoretical analysis which is evaluated in section 3.2. Parameters of the Monte-Carlo simulation is chosen as, $N = 1000$ packet number for one simulation, $N_s = 2$ repetition rate of the monocycles for one bit, and $\eta = 0.9$ efficiency of the photo-detector. Fading changes for every 200 symbol period.

For weak turbulence regime $\mu_x = 0$ and σ_x is chosen as 0.3, 0.37, 0.44 and 0.57 which corresponds to $\sigma_{SI}^2 = \{0.095, 0.15, 0.209, 0.380\}$ in terms of scintillation index. As seen in the figure 3.5 simulation results represented with solid-lines and theoretical results represented with dashed-lines have a good aligment with the help of Gauss-Hermite expansion.

For moderate turbulence condition, α and β parameters are chosen as $(4.16, 2.21)$,

$(4.00, 1.75)$ and $(4.05, 1.51)$ which corresponds to $\sigma_{SI}^2 = \{0.8, 0.96, 1.07\}$. Theoretical and simulation results are also have well alignment for all regions of moderate turbulence. For strong turbulence, unit mean light intensity is considered which corresponds to $\sigma_{SI}^2 = 1$.

Notice that as expected increasing scintillation index parameter from $\sigma_{SI}^2 = 0.1$ to 1 decreases the error performance smoothly. In the moderate and strong turbulence regions channel performance highly degrades. In order to avoid this performance penalty a simple convolutional code can be applied to the system or channel can switch from FSO to RF with a data rate penalty.

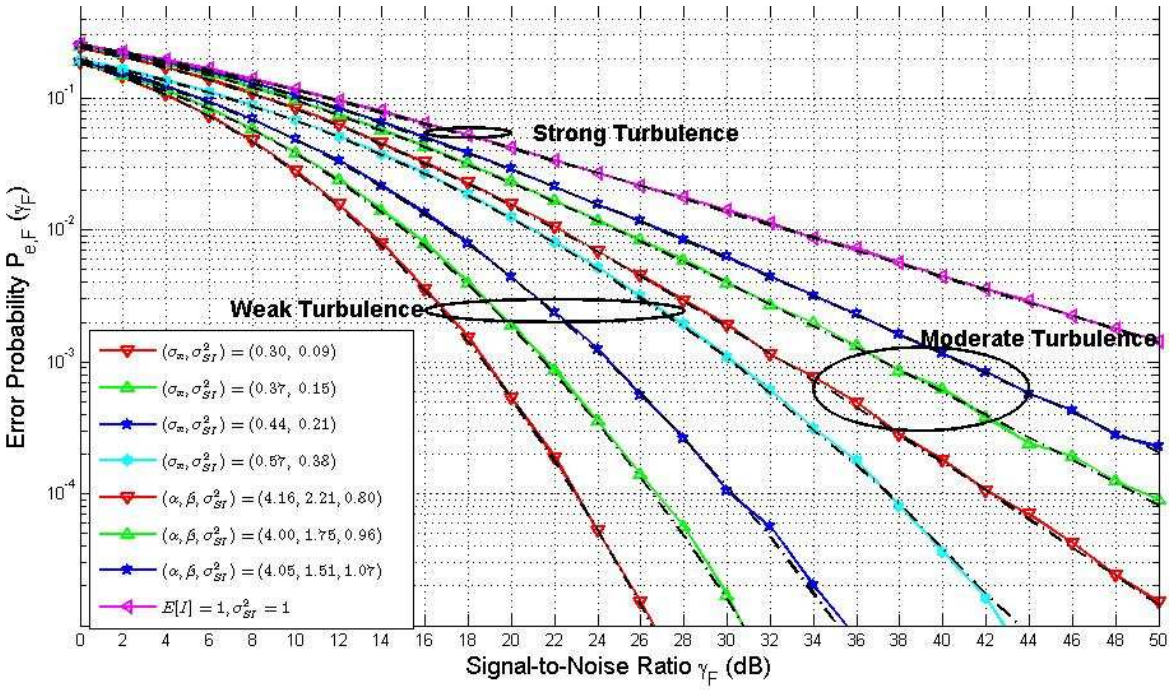


Figure 3.5. Comparision of the simulated and theoretical DEP's for weak, moderate and strong turbulence fading conditions

4. Multiuser Detection of IR FSO links

Proposed system distributes data to the endusers over FSO link. Thus, multiuser effect should be analyzed for the FSO channel.

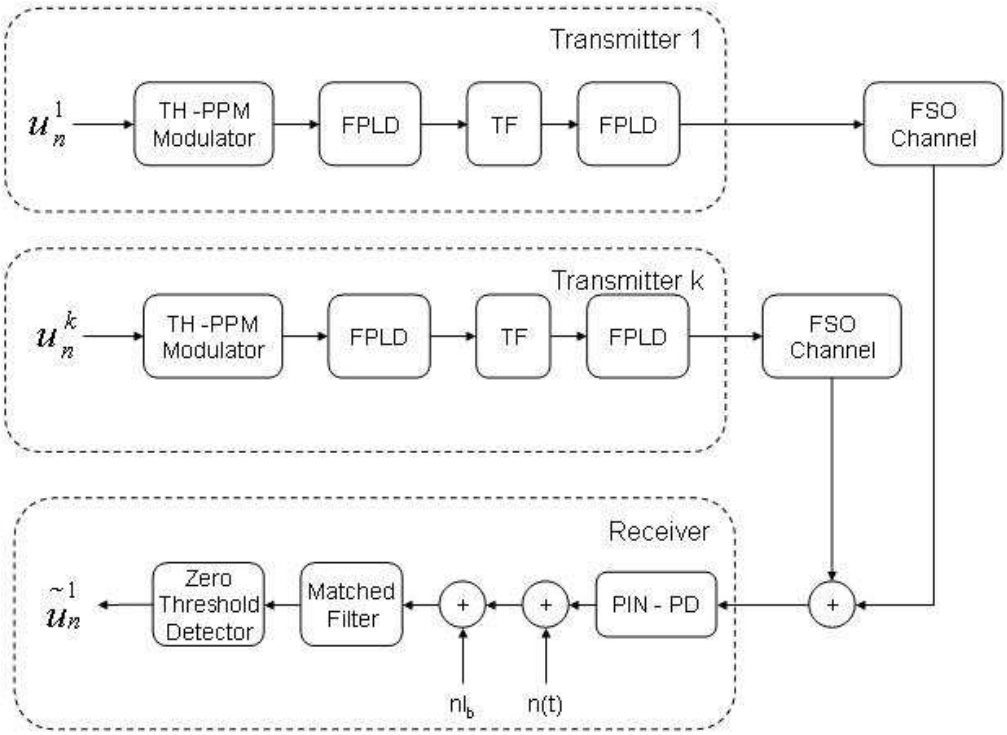


Figure 4.1. Proposed system for multiuser communication

Perfect power control are assumed for different users. Simple detection algorithms which are;

- Single user matched filter for asynchronous case
- Single user matched filter for synchronous case
- Decorrelating detection

will be analyzed in the following sections.

4.1. Single User Matched Filter Detection

In this section the UWB FSO link performance under multiuser interference is analysed for single user matched filter. Assuming all users are transmitted over different channels with identical and independent fading and perfect power control received signal from all users can be written as

$$r_{M_FSO}(t) = \eta I^{(1)} x_{FSO}^{(1)}(t) + \eta \sum_{k=2}^{N_u} I^{(k)} x_{FSO}^{(k)}(t - \tau^{(k)}) + n(t) \tag{4.1}$$

here $r_{M_FSO}(t)$ is the signal at the output of photodetector with multiuser interference and gauss noise. The main idea of the receiver is to extract the first user's signal using a matched filter. This method pretends the multiuser interference as an unknown noise.

Same correlator which is used for single user case will be used to extract the first user;

$$v(t) = p(t) - p(t - T_p) \tag{4.2}$$

where correlator output for the jth frame is

$$y(jT_f) = \int_{-\infty}^{\infty} r_{mFSO}(t) v(t - jT_f - c_j^{(1)} T_c) dt. \tag{4.3}$$

Correlator output is divided three parts where the first part is correlation of the first user for synchronious receiver shown as

$$y(jT_f)^{(1)} = \int_{-\infty}^{\infty} \eta I^{(1)} x_{FSO}^{(1)}(t) v(t - jT_f - c_j^{(1)} T_c) dt = \pm \eta I \sqrt{E_p} \tag{4.4}$$

and noise output is

$$y(jT_f)^{(n)} = \int_{-\infty}^{\infty} n(t) v(t - jT_f - c_j^{(1)} T_c) dt. \tag{4.5}$$

It can be easily shown that output is a gaussian distribution with mean is zero and variance is σ_n. Third part is the correlation of interfering users where the output for one interfering user is,

$$y(jT_f)^{(k)} = \eta I^{(k)} \sqrt{E_p} \sum_{j'=-\infty}^{\infty} \int_{-\infty}^{\infty} p\left(t - j'T_f - c_{j'}^{(k)} T_c - \tau^{(k)}\right) v(t - jT_f - c_j^{(1)} T_c) dt. \quad (4.6)$$

Defining the correlation function $R(x) = \int_{-\infty}^{\infty} p(t-x)v(t)dt$ a simpler equation can be written as

$$y(jT_f)^{(k)} = \eta I^{(k)} \sqrt{E_p} \sum_{j'=-\infty}^{\infty} R\left([j - j']T_f + [c_j^{(1)} - c_{j'}^{(k)}]T_c + d_{j'}^{(k)} T_d - \tau^{(k)}\right). \quad (4.7)$$

Here $\tau^{(k)}$ is the delay between user 1 and user k which spans many frames. Thus $\tau^{(k)}$ can be evaluated as

$$\tau^{(k)} = j_{1,k} T_f + \alpha_{1,k} \quad (4.8)$$

where $j_{1,k}$ is the time uncertainty of $\tau^{(k)}$ rounded to the nearest frame and $-T_f/2 \leq \alpha_{1,k} \leq T_f/2$ is the error in this rounding process. Then argument of the R(.) function can be rewritten as

$$[j - j' + j_{1,k}]T_f + [c_j^{(1)} - c_{j'}^{(k)}]T_c + d_{j'}^{(k)} + \alpha_{1,k}. \quad (4.9)$$

Assuming frame period as $T_f/2 \geq N_h T_c + 2T_d$ implies that $[c_j^{(1)} - c_{j'}^{(k)}]T_c + d_{j'}^{(k)} + \alpha_{1,k} \leq T_f - T_d$ which means there is only one frame of user k interfering to the one frame of user 1 as shown in the figure 4.2.

Regarding the fact that R(x) is nonzero only for $|x| \leq T_d$ correlator output can be simplified by setting $j - j' + j_{1,k} = 0$ which becomes

$$y_i(jT_f)^{(k)} = \eta I^{(k)} \sqrt{E_p} R\left([c_j^{(1)} - c_{j'}^{(k)}]T_c + d_{j'}^{(k)} T_d - \alpha_{1,k}\right) \quad (4.10)$$

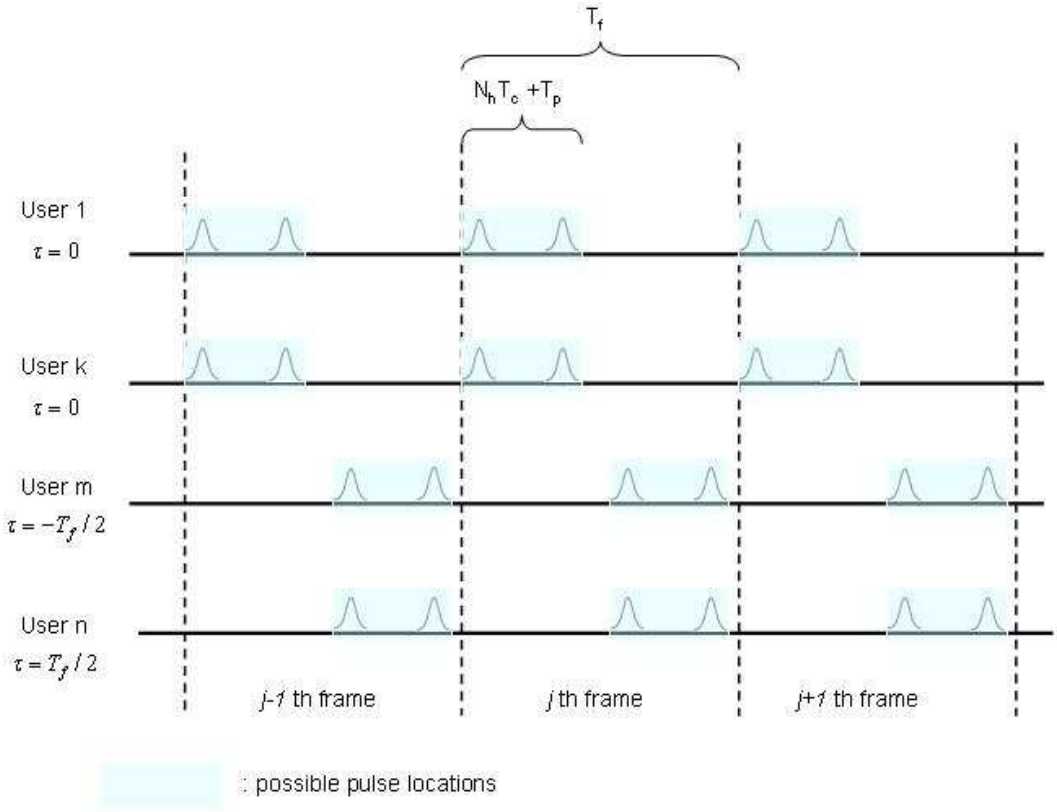


Figure 4.2. Pulse positions of the first user and an interfering user with 0, min, max time delays.

gives us the interference to jth frame of user 1 from user k.

4.1.1. Gauss Model

If the time uncertainty $\tau^{(k)}$ is assumed uniformly distributed between $-T_f/2$ and $T_f/2$, then the probability density function can be written as

$$p_{\alpha_{1,k}}(z) = \begin{cases} T_f^{-1}, & -T_f/2 \leq x < T_f/2 \\ 0, & \text{otherwise.} \end{cases} \tag{4.11}$$

Thus, expectation of the interference to one frame over $\tau^{(k)}$ can be shown as [9],

$$E\{y_i(jT_f)\} = \eta E\{I\}\sqrt{E_p}T_f^{-1} \int_{-T_f/2+[c_j^{(1)}-c_{j+j_{1,k}}^{(k)}]T_c+d_{j+j_{1,k}}}^{T_f/2+[c_j^{(1)}-c_{j+j_{1,k}}^{(k)}]T_c+d_{j+j_{1,k}}} R(\varsigma)d\varsigma. \tag{4.12}$$

Integration limits can be expand to infinity when $T_f/2 \geq N_hT_c + 2T_d$ and $R(x) \neq 0$ only for $|x| \leq T_p$ criteria applies since

$$R(x) = \begin{cases} 0, & x < -T_f/2 + [c_j^{(1)} - c_{j+j_{1,k}}^{(k)}]T_c + d_{j+j_{1,k}} \\ 0, & x > T_f/2 + [c_j^{(1)} - c_{j+j_{1,k}}^{(k)}]T_c + d_{j+j_{1,k}}. \end{cases} \tag{4.13}$$

Expectation of the interference simplifies to

$$E\{y_i(jT_f)\} = \eta E\{I\}\sqrt{E_p}T_f^{-1} \int_{-\infty}^{\infty} R(\varsigma)d\varsigma \tag{4.14}$$

which equals to 0. Similarly second moment of the interference is variance of the uniformly distributed interference from the kth user and can be calculated as

$$E\{|y_i(jT_f)|^2\} = E\{|I|^2\}(\eta)^2E_pT_f^{-1} \int_{-\infty}^{\infty} |R(\varsigma)|^2d\varsigma = \sigma_I^2\eta^2E_p\sigma_{self}^2 \tag{4.15}$$

where σ_I^2 is the variance of turbulence fading.

In the proposed system, there exists N_u users in the channel, thus $N_u - 1$ indepen-

dent frame will interfere to the one frame of the user 1. It is reasonable to assume total interference distribution is gaussian for high increasing user number from the central limit theorem. Thus, total noise at the correlator output can be found as summation of two gaussian distribution which are background noise and multiuser interference. Signal to noise ratio at the output of the correlator for one frame can be shown as

$$SNR_f = \frac{\left(\eta I^{(1)}\right)^2 E_p}{N_0 + (N_u - 1)\sigma_I^2 \eta^2 E_p \sigma_{self}^2}. \tag{4.16}$$

Also it is assumed that interference from different frames is independent due to the fact that interframe correlation is smaller compared to self correlation. One bit is summation of N_s frames and bit SNR is

$$SNR_b = \frac{N_s \left(\eta I^{(1)}\right)^2 E_p}{N_0 + (N_u - 1)\sigma_I^2 \eta^2 E_p \sigma_{self}^2}. \tag{4.17}$$

For single user matched receiver correlator output is fed to a simple zero threshold detector and the result error probability for the asynchronous case is

$$\begin{aligned} P_{b_async}(\gamma_p, N_u, I) &= Q\left(\sqrt{\frac{N_s \left(\eta I^{(1)}\right)^2 E_p}{N_0 + (N_u - 1)\sigma_I^2 \eta^2 E_p \sigma_{self}^2}}\right) \\ &= Q\left(\sqrt{\frac{\left(\eta I^{(1)}\right)^2 \gamma_p}{1 + \frac{(N_u - 1)\sigma_I^2 \eta^2 \gamma_p \sigma_{self}^2}{N_s}}}\right) \end{aligned} \tag{4.18}$$

Under weak turbulence conditions the light intensity is lognormal distributed and the error probability can be calculated using the Gauss-Hermite expression as,

$$P_{b_async_weak}(\gamma_p, N_u) = \frac{1}{2\sqrt{\pi}} \sum_{i=1}^{n} \omega_i erfc\left(\sqrt{\frac{\left(\eta I_0 e^{y_i\sqrt{8\sigma_x^2} + 2m_{u_x}}\right)^2 \gamma_p}{2 + 2\frac{(N_u - 1)\sigma_I^2 \eta^2 \gamma_p \sigma_{self}^2}{N_s}}}\right) \tag{4.19}$$

Moderate turbulence is another region applied to the FSO channels where the fading effects are more severe than weak turbulence. Moderate turbulence is modeled

using gamma-gamma distribution. Error performance can be shown as

$$P_{b_async_mod}(\gamma_p, N_u) = \frac{2^{\alpha+\beta-3}}{\sqrt{\pi^3}\Gamma(\alpha)\Gamma(\beta)} \times G_{5,2}^{2,4}\left[\frac{8\eta^2 N_s \gamma_p}{\alpha^2\beta^2(1+\frac{(N_u-1)\sigma_I^2\eta^2\gamma_p\sigma_{self}^2}{N_s})}\middle| \begin{matrix}\frac{1-\alpha}{2}, \frac{2-\alpha}{2}, \frac{1-\beta}{2}, \frac{2-\beta}{2}, 1 \\ 0, \frac{1}{2}\end{matrix}\right]. \quad (4.20)$$

However, uncorrelated frames for one bit is not a valid assumption. In 4.3 it can be easily seen that gaussian assumption is accurate while repetition rate N_s is equal to 1. Increasing repetition number decreases the accuracy as seen in the figure 4.4

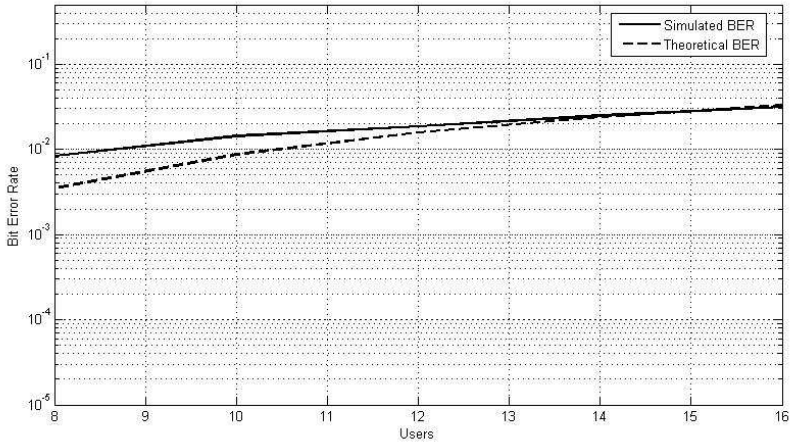


Figure 4.3. Average BER of the TH-PPM UWB system versus user number for a repetition code with $N_s = 1$

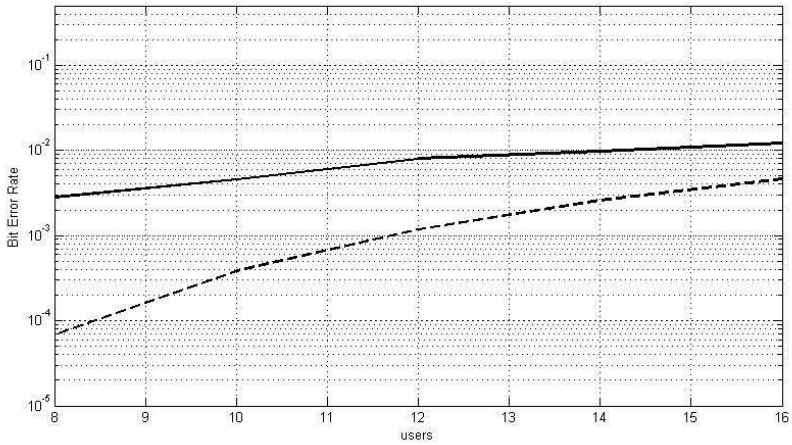


Figure 4.4. Average BER of the TH-PPM UWB system versus user number for a repetition code with $N_s = 2$

4.1.2. Accurate model

Since adjacent frames of a bit is not independent we should model interference to one bit instead of one frame. Assuming interfering user data does not change during one bit period, bit interference to user 1 at $0th$ bit can be shown as

$$y_i(jT_f) = \eta I \sqrt{E_p} \sum_{k=2}^{N_u} \left[\sum_{j=0}^{N_s-1} R_w(\Theta_{0,j}^{(k)}) \right] \tag{4.21}$$

where

$$\Theta_{0,j}^{(k)} = \alpha_k + c_j^{(k)} T_c + d_0^{(k)} T_d \tag{4.22}$$

$d_0^{(k)}$ represents the $0th$ bit of the user k. The probability density function (pdf) of $\Theta_{0,j}^{(k)}$ conditioned on $d_0^{(k)}$ and α_k becomes

$$f_{\Theta_0 d,\alpha}\left(\Theta | d_0^{(k)} = d, \alpha_k = \alpha\right) = \frac{1}{N_h} \sum_{h=0}^{N_h-1} \delta_D(\Theta - hT_c - dT_d - \alpha). \tag{4.23}$$

The characteristic function of $R(\Theta_{0,j}^{(k)})$ conditioned on $d_0^{(k)}$ and α_k is

$$\begin{aligned} \Phi_{R|d,\alpha,I}(\omega) &= E\left[e^{j\omega\eta I\sqrt{E_p}R} | d_0^{(k)} = d, \alpha_k = \alpha, I \right] \\ &= \frac{1}{N_h} \sum_{h=0}^{N_h-1} e^{j\omega\eta I\sqrt{E_p}R(\alpha + hT_c + dT_d)} \end{aligned} \tag{4.24}$$

Further we can define interference to one bit from user k as $X^{(k)} = \eta I \sqrt{E_p} \sum_{j=0}^{N_s-1} R_w(\Theta_{0,j}^{(k)})$. Then conditional characteristic function of $X^{(k)}$ is obtained as

$$\begin{aligned} \Phi_{X^{(k)}|d,\alpha,I}(\omega) &= E\left[e^{j\omega\eta I\sqrt{E_p}\sum_{j=0}^{N_s} R(\Theta_{0,j}^{(k)})} | d_0^{(k)} = d, \alpha_k = \alpha, I \right] \\ &= \left(\frac{1}{N_h} \sum_{h=0}^{N_h-1} e^{j\omega\eta I\sqrt{E_p}R(\alpha + hT_c + dT_d)} \right)^{N_s} \end{aligned} \tag{4.25}$$

where the second equality follows from the fact that $R(\Theta_{0,j}^{(k)}), j = 0, ..., N_s$ are independent when conditioned on $d_0^{(k)}$, I and α. Since our assumption is that the pseudorandom TH sequence is random for all frames. Then the CF of $X^{(k)}$ conditioned α_k and I can be obtained using the theorem of total probability as

$$\begin{aligned}\Phi_{X^{(k)}|\alpha,I}(\omega) &= \Phi_{X^{(k)}|0,\alpha,I}(\omega)Pr(d=0) + \Phi_{X^{(k)}|1,\alpha,I}(\omega)Pr(d=1) \\ &= \frac{1}{2N_h^{N_s}}\Bigg[\left(\sum_{h=0}^{N_h-1} e^{j\omega\eta I\sqrt{E_p}R(\alpha+hT_c)}\right)^{N_s} \\ &\quad + \left(\sum_{h=0}^{N_h-1} e^{j\omega\eta I\sqrt{E_p}R(\alpha+hT_c+\delta)}\right)^{N_s}\Bigg]. \end{aligned} \tag{4.26}$$

Averaging out α_k, we obtain the CF of the kth interferer as

$$\Phi_{X^{(k)}|I}(\omega) = \frac{1}{T_f}\int_{-T_f/2}^{T_f/2} \Phi_{X^{(k)}|\alpha,I}(\omega)d\alpha \tag{4.27}$$

Assuming the interference from different users are independent, the CF of the total interference conditioned fading is

$$\Phi_{X|I}(\omega) = \prod_{k=2}^{N_u} \Phi_{X^{(k)}|I}(\omega). \tag{4.28}$$

Finally, the CF of the total interference by averaging out I can be found as

$$\Phi_X(\omega) = \int_0^\infty \Phi_{X|I}(\omega)f_I(I)dI. \tag{4.29}$$

Since the background noise is independent from interference CF of total noise $\Phi_\Lambda(\omega)$ can be defined as product of interference and background noise. Therefor the average bit error probability for the desired user is [10]

$$P_{b_precise} = \frac{1}{2} - \frac{1}{\pi}\int_0^\infty \frac{sin(N_sR(0)\omega)}{\omega}\Phi_\Lambda(\omega)d\omega. \tag{4.30}$$

4.1.3. Synchronous gauss model

In the proposed system, all users will use the same FSO channel between base station and central station. Frame synchronous case is analyzed in this section. Time uncertainty α set 0 for all users to be synchronized with user 1 which is also synchronized with the receiver. Recalling the same assumption with asynchronous case, multiuser interference is assumed as gauss distributed. Figure 4.5 shows the distribution of multiuser interference at the output receiver correletor which is matched to the first user and no turbulence fading effect is applied to the channel. Also histogram of a gauss distributed random variable is plotted in the same figure with variance same as the interference. Therefore, gauss assumption is validated by simulation. And fig-

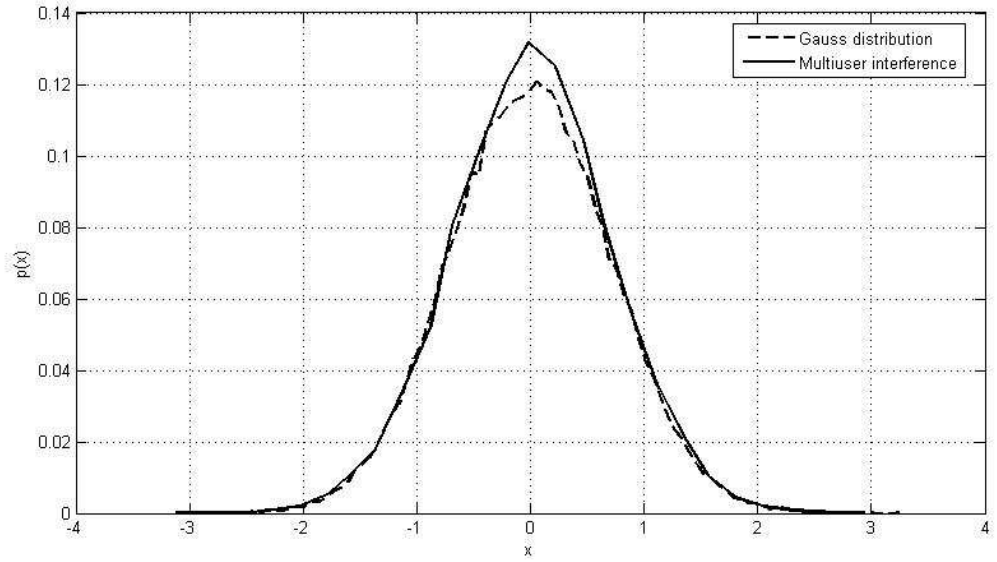


Figure 4.5. Distribution of multiuser interference with 8 users and no turbulence fading at the output of correlator and gauss distribution with the same variance

ure 4.6 shows the distribution of multiuser interference with weak turbulence fading is applied to the channel. Distribution does not match as good as no fading case but it is still an accurate assumption. Notice that distribution of the multiuser interface is a discrete distribution since the time hopping codes are discrete. Thus, normalized gauss distributions and the interference distribution have different heights despite their similar distribution shapes and variances. In order to easily show the similarity of the shapes, distributions are amplified to the same height in the plot. Finally figure

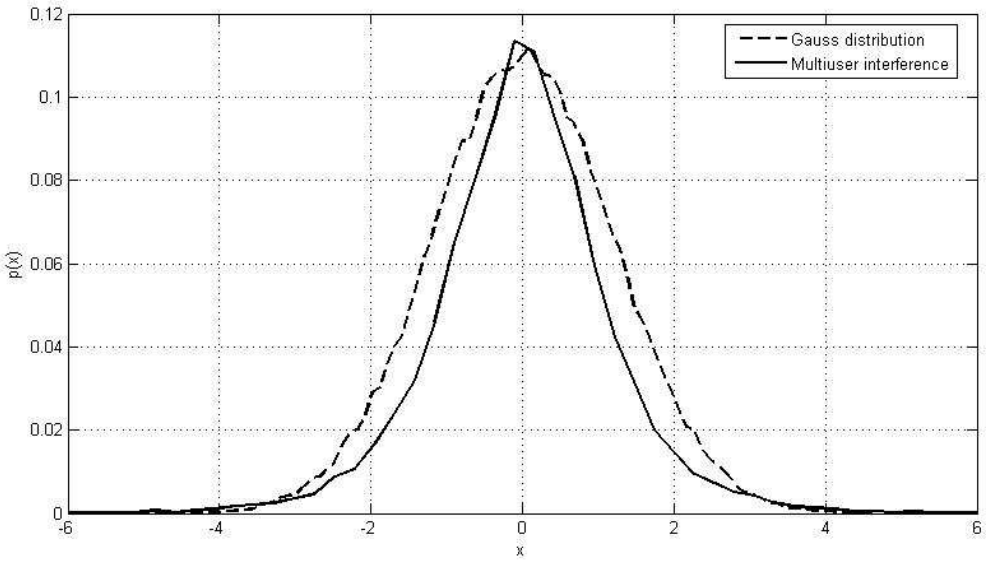


Figure 4.6. Distribution of multiuser interference with 8 users and weak turbulence fading at the output of correlator and gauss distribution with the same variance

4.7 shows the distribution for moderate turbulence fading which is similar to weak turbulance case. Result interference for synchronous system can be shown as

$$y_i(jT_f)^{(k)} = \eta I \sqrt{E_p} R \left([c_j^{(1)} - c_{j'}^{(k)}] T_c + d_{j'}^{(k)} T_d \right) \tag{4.31}$$

and using the same methodology with synchronous channel analysis second moment of the interference can be calculated as

$$E_{c,d}\{|y_i(jT_f)|^2\} = (\eta I)^2 E_p E\{|R(\varsigma)|^2\} = E\{|I|^2\}(\eta)^2 E_p \sigma_{self}^2 \tag{4.32}$$

where

$$E\{|R\left([c_j^{(1)} - c_{j'}^{(k)}] T_c + d_{j'}^{(k)} T_d \right)|^2\} = \frac{1}{N_h} \tag{4.33}$$

Therefor the bit error probability for synchronous channel is expressed as

$$P_{b_gauss}(I) = Q\left(\sqrt{\frac{N_s (\eta I)^2 E_p}{N_0 + \frac{(N_u - 1)\sigma_I^2 \eta^2 E_p}{N_h}}} \right). \tag{4.34}$$

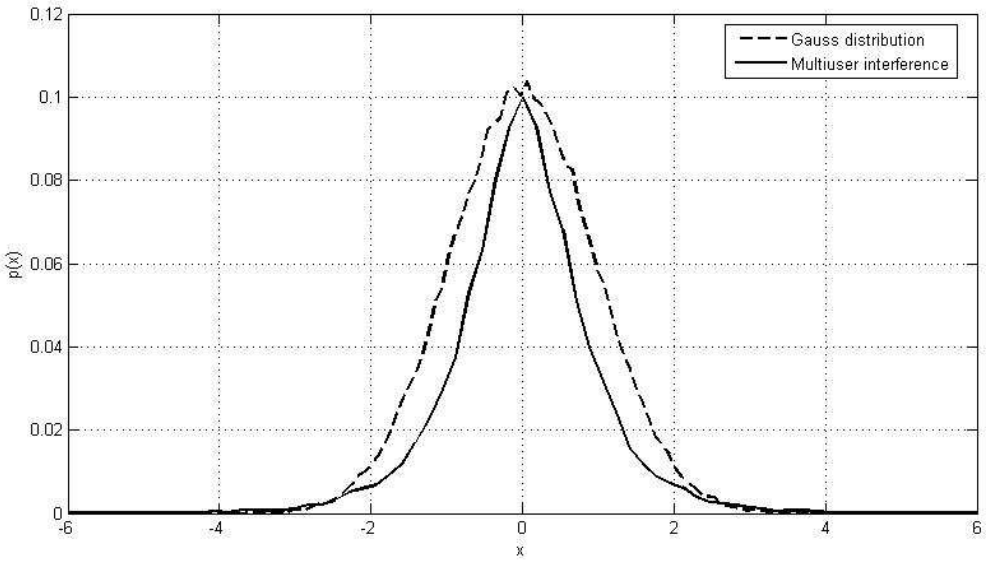


Figure 4.7. Distribution of multiuser interference with 8 users and moderate turbulence fading at the output of correlator and gauss distribution with the same variance

Under weak turbulence conditions, the error probability can be expressed using Gauss-Hermite expression as

$$P_e(\gamma_p, N_u) = \frac{1}{2\sqrt{\pi}} \sum_{i=1}^{n} \omega_i erfc\left(\sqrt{\frac{(\eta I_0 e^{y_i \sqrt{8\sigma_x^2} + 2\mu_x})^2 \gamma_p}{2 + 2\frac{(N_u - 1)\sigma_I^2 \eta^2 \gamma_p}{N_s N_h})}} \right). \tag{4.35}$$

Similar to the asynchronous case,the error probability under moderate turbulence can be shown as

$$\begin{aligned} P_{e,mod}(\gamma_p, N_u) &= \int_0^\infty \frac{1}{2} erfc\left(\sqrt{\frac{\gamma_p(\eta I^2)}{2 + \frac{2(N_u - 1)\sigma_I^2 \gamma_p \eta^2}{N_s N_h}}} \right) \\ &\times \frac{2(\alpha\beta)^{\frac{\alpha+\beta}{2}}}{\Gamma(\alpha)\Gamma(\beta)} I^{\frac{\alpha+\beta}{2}-1} K_{\alpha-\beta}\left(2\sqrt{\alpha\beta I}\right) dI \end{aligned} \tag{4.36}$$

which has a closed form solution using the Meijer G function [11] given by

$$\begin{aligned} P_{b_gauss_mod}(\gamma_p, N_u) &= \frac{2^{\alpha+\beta-3}}{\sqrt{\pi^3}\Gamma(\alpha)\Gamma(\beta)} \\ &\times G_{5,2}^{2,4}\left[\frac{8\eta^2 N_s \gamma_p}{\alpha^2\beta^2(1+\frac{(N_u-1)\sigma_I^2\eta^2\gamma_p}{N_h N_s})}\middle| \begin{matrix} \frac{1-\alpha}{2}, \frac{2-\alpha}{2}, \frac{1-\beta}{2}, \frac{2-\beta}{2}, 1 \\ 0, \frac{1}{2} \end{matrix}\right]. \end{aligned}$$

4.2. Synchronous Decorrelating Detection

Decorrelating detection is a simple linear CDMA multiuser detector. This method can be used for TH coded multiuser channels [24].

The output vector of the bank of K matched filter outputs can be written as

$$\mathbf{y} = \mathbf{RAb} + \mathbf{n} \tag{4.37}$$

where $\mathbf{n}$ is a Gaussian random vector, $\mathbf{R}$ is the covariance matrix of the user TH codes, $\mathbf{A}$ is the Amplitudes of the users and $\mathbf{b}$ is the data vector.

We can generate $\mathbf{R}$ matrix for TH coded users as;

$$\mathbf{R}_{mn} = \frac{1}{N_s}\int_0^{T_f} \sum_{j=1}^{N_s} p_r(t - c_j^{(k)} T_c) \sum_{k=1}^{N_s} p_r(t - c_k^{(n)} T_c) dt \tag{4.38}$$

If we premultiply the vector of matched filter outputs by $\mathbf{R}^{-1}$

$$\mathbf{R}^{-1}\mathbf{y} = \mathbf{R}^{-1}\mathbf{RAb} + \mathbf{R}^{-1}\mathbf{n} = \mathbf{Ab} + \mathbf{R}^{-1}\mathbf{n}. \tag{4.39}$$

Notice that the kth component of (13) is free from the interference caused by other users. The only source of interference is the background noise multiplied with

inverse of the covariance matrix. And the variance of the noise is

$$\begin{aligned} E[(\mathbf{R}^{-1}\mathbf{n})(\mathbf{R}^{-1}\mathbf{n})^T] &= E[\mathbf{R}^{-1}\mathbf{n}\mathbf{n}^T\mathbf{R}^{-1}] \\ &= \sigma^2\mathbf{R}^{-1}\mathbf{R}\mathbf{R}^{-1} = \sigma^2\mathbf{R}^{-1} \end{aligned} \tag{4.40}$$

Regarding the background noise, probability of error for the FSO channel can be rewritten as

$$P_e(\gamma_p) = \frac{1}{2\sqrt{\pi}} \sum_{i=1}^{n} \omega_i erfc\left(\sqrt{\frac{(\eta I_0 e^{y_i\sqrt{8\sigma_x^2}+2\mu_x})^2\gamma_p}{2R_{kk}^{+}}}\right) \tag{4.41}$$

where R_{kk}^{+} is the kkth element of the $\mathbf{R}^{-1}$.

4.3. Simulation Results

In this section, simulation results of the proposed system's multiuser performance is shown and they are compared with the theoretical evaluations given in chapter 4. Perfect power control is assumed on the channel thus, bit energy for all users is taken as E_b which is equal to 1 at the receiver input. Simulation parameters are chosen as $N_s = 2$ for monocycle repetition for one bit, $N_h = 10$ for maximum time hopping delay.

Figure 4.8 gives the synchronous system performance under no turbulence fading case which is given for the comparison purposes with fading cases.

Simulation and theoretical results of an FSO channel's BER curve under weak turbulence ($\sigma^2 = 0.37$) with $N_u = 1, 4, 8$ users is plotted in figure 4.9. Note that simulated BER curve does not match to the theoretical curve for multiuser case. However, increasing the user number decreases the gap between simulation and theory. This result indicates that the number of pulses traveling over the air interface is not sufficient for guaranteeing the validity of the gaussian approximation for the interference noise.

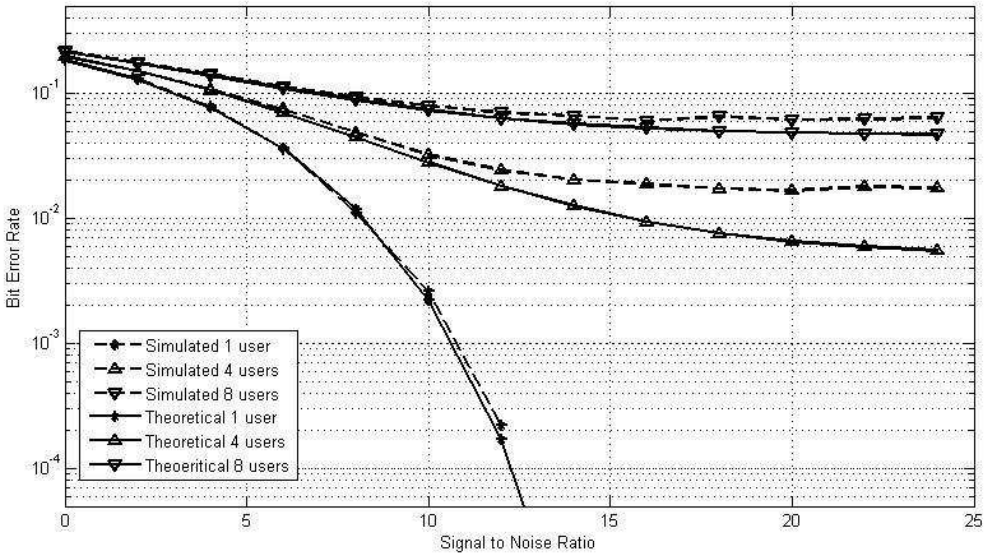


Figure 4.8. Synchronous multiuser FSO performance with no fading

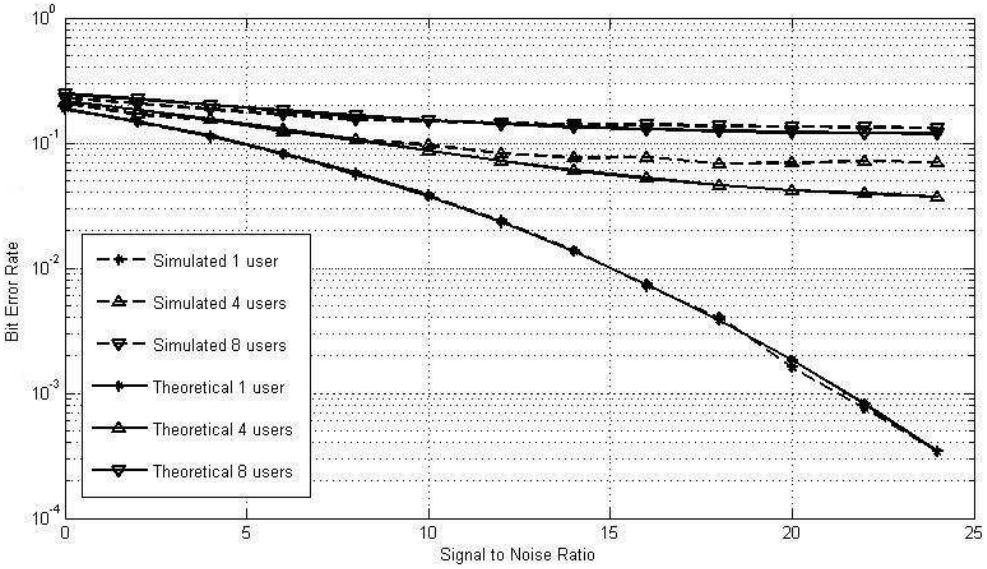


Figure 4.9. Synchronous multiuser FSO performance under weak turbulence

Also weak turbulance case is simulated in figure 4.10 for the case that all users use the same channel that means fading will be same for all users. It is easily seen that error performance is increased when the fading is not independent between users.

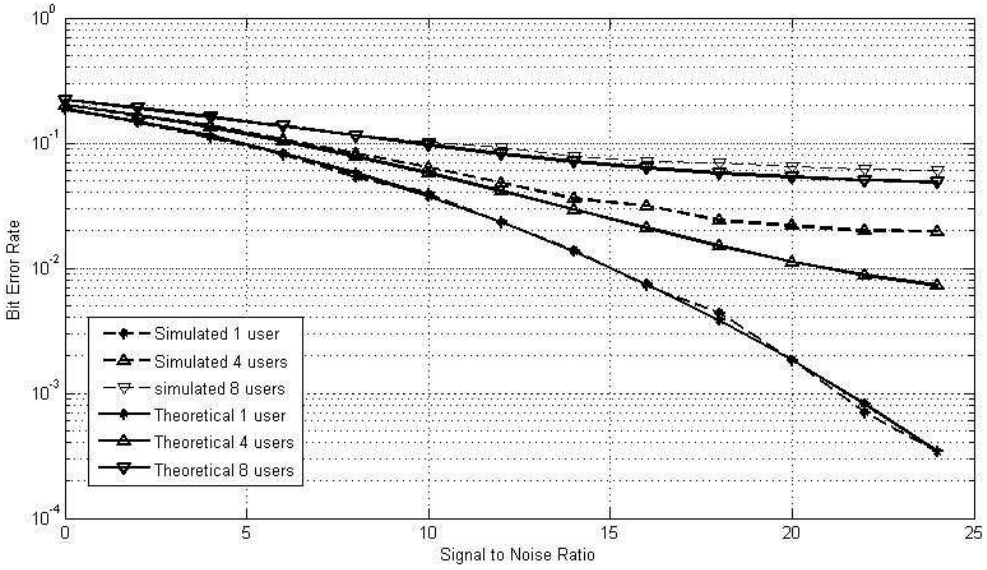


Figure 4.10. Synchronous multiuser FSO performance under weak turbulence when the same channel is used by all users

Figure 4.11 shows BER curve under moderate turbulence $\{\alpha = 4, \gamma = 1.75\}$ for uncorrelated channel variance. User numbers are chosen as $N_u = \{1, 4, 8\}$. Simulation results and theoretical results which are derived via Meijer G functions are well matched.

As seen in the figures turbulence fading decreases the multiuser performance dramaticly especially for the independent fading cases. Figure 4.12 shows the decorreleting detector error performance under weak turbulence ($\sigma^2 = 0.1$) with parameters $N_s = 6$ and $N_h = 4$ and multiuser interference affects are perfectly filtered with this type of detector. However, decorrelating detector has a very high complexity penalty since it requires matrix inversion for every frame.

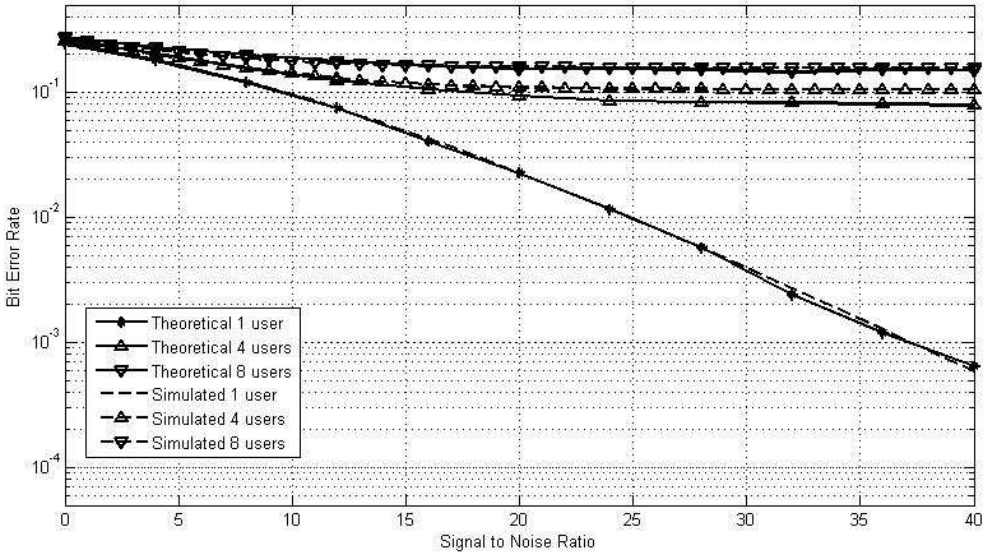


Figure 4.11. Synchronous multiuser FSO performance under moderate turbulence

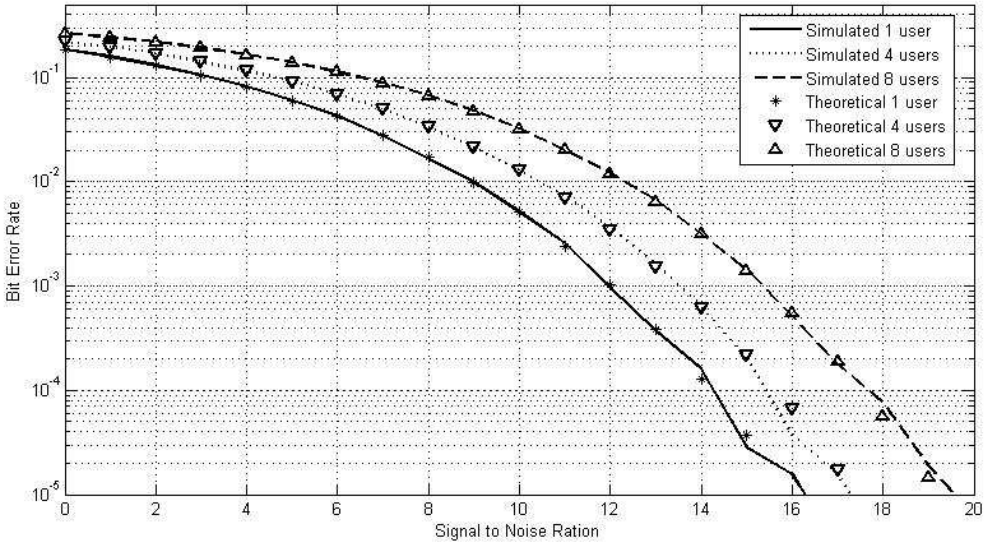


Figure 4.12. Decorrelating Detector performance

5. CONCLUSIONS

In this thesis, a simple system is proposed to increase the RF UWB coverage using free space optical channels. First of all gaussian pulse is chosen as the pulse type due to the positive constraint of the direct detection method of the optical channels. UWB pulse train is modulated via time hoping pulse position modulation method due to it's simplicity and no negative component requirement. In order to generate optical signal Optical impulse radio system is used due to it's simplicity. Other optical generation methods can be evaluated for FSO as a future work. System performance for single user case is simulated and theoretically analyzed in weak, moderate and strong atmospheric turbulence regimes.

In the analyses of single user a simple matched filer is used at the receiver which is designed for PPM modulation. It is seen that the system provides very high relaibilty for the weak turbulance regimes. However, system performance is highly degraded in the moderate and strong turbulence regimes. In order to increase the system performance a simple convolutional code can be applied to the system or switching FSO channel to an RF channel in the strong turbulence regime can be studied as another future work.

Also multiuser performance of the system is analyzed for asynchronous and synchronous cases in weak and moderate turbulance regimes. It is seen that independent fading blocks reliable data transfer with single user matched detector in multiuser mode especially for the synchronous case. Thus, decorrelting detection algorithm which is used for CDMA detection is analysed and simulated for TH system.

In conclusion, fast and cheap deployment characteristics of the FSO channels perform a good alternative to the fiber channels for the distribution of UWB signals in the urban areas.

APPENDIX A: DERIVATION OF EQUATION (3.12)

Gauss Hermite quadrature or Gauss Hermite expansion is a method for approximating the value of integrals of the following kind

$$\int_{-\infty}^{\infty} e^{-x^2} f(x) dx \tag{A.1}$$

into n point finite sum

$$\int_{-\infty}^{\infty} e^{-x^2} f(x) dx \approx \sum_{i=1}^{n} \omega_i f(x_i) \tag{A.2}$$

where n is the number of sample points to use for the approximation[12]. This approximation is used to find closed form of the error probabilty evaluation for weak turbulance fading. Equation 3.11 can be rewritten by the change of parameters as

$$P_e(\gamma_p) = \frac{1}{2\sqrt{\pi}} \int_{-\infty}^{\infty} erfc\left(\sqrt{N_s \gamma_p (\eta I_0 e^{y\sqrt{8\sigma_x^2}})^2/2}\right) e^{-y^2} dy \tag{A.3}$$

and using the expansion equation 3.12 can be calculated as

$$P_e = \frac{1}{2\pi} \sum_{i=1}^{n} \omega_i erfc\left(\sqrt{\frac{N_s \gamma_p (\eta I_0 e^{y_i\sqrt{8\sigma_x^2}})}{2}}\right). \tag{A.4}$$

REFERENCES

1. Moshe Ran, Yossef Ben Ezra, Motti Haridim, and Boris. I. Lembrikov, "Ultra wideband radio over optical fiber" *Wireless World Research Forum*, Vol. 21, March 2007.

2. Tom Garlington, Joel Babbitt, and George Long, "Analysis of free space optics as a transmission technology" *U.S. Army Information Systems Engineering Command*, No. AMSEL-IE-TS-05001, March 2005.

3. Kamran Kiasaleh, "Performance of APD-Based, PPM free-space optical communication systems in atmospheric turbulence" *IEEE Transactions on Communications,*, Vol. 53, No. 9, September 2005.

4. Xiaoming Zhu and Joseph M. Kahn, "Free-Space Optical Communication Through Atmospheric Turbulence Channels" *IEEE Transactions on Communications,*, Vol. 50, No. 8, August 2002.

5. Weihua Zhuang, Xuemin (Sherman) Shen, Qi Bi "Ultra-wideband wireless communications" *Wirel. Commun. Mob. Comput.*, Vol. 149, No. 3, pp. 663-685 2003.

6. Chen X, Kiaei S. "Monocycle shapes for ultra-wideband system" *Proceedings of IEEE ISCAS*, pp. 597-600 2002.

7. K Dridi, H. Hamam, "Optical generation of UWB signal: a comparative study" *IEEE International Conference on Signal Processing and Communications*, No. 1, pp. 1155-1158 Nov. 2007.

8. Wen Piao Lin, Jun Yu Chen, "Implementation of a new ultrawideband impulse system" *IEEE photonics technology letters*, Vol. 17, No. 11, pp. 2418-2420 Nov. 2005.

9. Moe Z. Win and Robert A. Scholtz, "Ultra-Wide Bandwidth Time-Hopping Spread-Spectrum Impulse Radio for Wireless Multiple-Access Communications", *IEEE Trans. Commun.*, vol. 48, pp. 679-690, Apr. 2000.

10. Bo Hu and Norman C. Beaulieu, "Precise bit error rate of TH-PPM UWB systems in the presence of multiple access interference", *IEEE Conference on Ultra Wideband Systems and Technologies* , pp. 106-110, Nov. 2003.

11. Abdelmoula Bekkali, Pham Tien Dat, Kamugisha Kazaura, Kazuhiko Wakamori and Mitsuji Matsumoto, "Performance analysis of SCM-FSO links for transmission of CDMA signals under gamma-gamma turbulent channel", *IEEE Military Communications Conference*, pp. 1-5, Oct. 2009.

12. M. Abramowitz and I. A. Stegun, *Handbook of Mathematical Functions with Formulas, Graphs, and Mathematical Tables*, 10th ed. New York: U.S. Department of Commerce, Dec. 1972.

13. ECMA-368, "High Rate Ultra Wideband PHY and MAC Standard," Dec. 2005.

14. Fei Zeng and Jianping Yao, "An Approach to All-Optical UWB Pulse Generation", *in Proc. IEEE Int. Topical Meeting Microw. Photon. (MWP'06)*, pp. 13 2006

15. Carlsson C., Larsson A.,Alping A., "RF transmission over multimode fibers using VCSELs comparing standard and high - bandwidth multimode fibers," *Journ. of Lightwave Technol.*, vol.22, no. 7, pp. 1694-1700, July 2004.

16. Anthony Acampora, "Last Mile by Laser" *Scientific American*, July 2002.

17. J. Derenick, C. Thorne and J. Spletzer, "Hybrid Free-space Optics/Radio Frequency (FSO/RF) Networks for Mobile Robot Teams" *Multi-Robot Systems: From Swarms to Intelligent Automata*, Alan C. Schultz and Lynne E. Parker Eds., New York, NY, Springer, 2005.

18. I. Kim and E. Korevaar, "Availability of Free Space Optics (FSO) and Hybrid

FSO/RF Systems" *Optical Wireless Communications IV*, August 2001.

19. A. Akbulut, G. Ilk, and F. Ari. "Design, availability and reliability analysis on an experimental outdoor FSO/RF communication system." *In Proc. Intern. Transparent Optical Networks Conf. (ICTON)*, pp. 403-406, July 2005.

20. I. Guvenc and H. Arslan, "On the Modulation Options for UWB Systems." *Proc. IEEE MILCOM 03*, pp. 892-897., Oct. 2003.

21. R. C. Qiu, H. Liu, X. Shen, "Ultra-wideband for multiple access communications." *IEEE Communications Magazine,* , pp. 80-87, 2005.

22. G. Durisi, S. Benedetto, "Performance evaluation and comparison of different modulation schemes for UWB multiaccess systems." *in Proc. IEEE ICC-03*, vol. 3 pp. 2187-2191, May 2003.

23. John G. Proakis, Masoud Salehi, *Digital Communications*, New York: McGraw-Hill, 2008.

24. Sergio Verdu, *Multiuser Detection*, Cambridge University Press, 1998.

25. S. M. Navidpour, M. Uysal, M. Kavehrad, "BER performance of free-space optical transmission with spatial diversity", *IEEE Trans. Wireless Commun.*,vol. 6 pp. 2813-2819 2007.

26. The Wolfram Function Site (2004), http://functions.wolfram.com/.

27. S. Karp, R. Gagliardi, S. E. Moran, and L. B. Stotts, *Optical Channels*. New York: Plenum, 1988.

28. A. Ishimaru, *Wave Propagation and Scattering in Random Media*. New York: Academic, 1978, vol. 12.

29. J. W. Goodman, *Statistical Optics*. New York: Wiley, 1985.

30. J. M. Kahn, J. R. Barry, "Wireless infrared communications" *in Proc. IEEE*, vol. 85, no. 2, Feb 1997